Review Article

phys. stat. sol. (b) **204**, 587 (1997)

Subject classification: 68.35.Bs; 61.10.Yh; 61.16.Ch; S5.11; S5.12

Discommensurate Reconstructions of (111)Si and Ge Induced by Surface Alloying with Cu, Ga and In

J. Zegenhagen[1]) (a), P. F. Lyman (b), M. Böhringer (c), and M. J. Bedzyk (b, d)

(a) Max-Planck-Institut für Festkörperforschung, Heisenbergstr. 1, D-70569 Stuttgart, Germany

(b) Department of Materials Science and Engineering and Materials Research Center, Northwestern University, Evanston, Illinois 60208, USA

(c) Université de Lausanne, Institute de Physique Expérimentale, CH-1015 Lausanne, Switzerland

(d) Materials Science Division, Argonne National Laboratory, Argonne, Illinois 60439, USA

(Received April 28, 1997)

Contents

---

[1]) Corresponding author: Tel.: +49 71 16 89 17 31, Fax: +49 71 16 89 17 12, e-mail: jorg@tunux2.mpi-stuttgart.mpg.de

1. Introduction

The termination of a bulk crystal by a free surface leads to the occurrence of unsaturated chemical bonds for the surface atoms corresponding to so-called dangling bonds for the case of a predominantly covalent material such as semiconductors. This frustrated chemistry of the clean surface is the driving force for reconstructions. Likewise in the case of adsorption on semiconductors the equilibrium structure is strongly dictated by the attempt to achieve chemical passivation. Owing to the strong and highly directional bonds of covalent semiconductors the ground state in energy of the resulting surface reconstruction is usually well ordered, periodic and commensurate with the bulk of the substrate. While the search is ongoing, a large number of adsorbate induced reconstructions fitting into this picture have meanwhile been discovered (see e.g. [1, 2]). However, some adsorbates do not fit this scheme and give rise to reconstructions which seem to be astonishingly different.

Already in 1964 Lander and Morrison [3] observed rather complex low-energy electron diffraction (LEED) patterns subsequent to the deposition of Al (covalent radius 1.26 Å) and In (covalent radius 1.44 Å) on Si(111) (Si covalent radius 1.17 Å). Lacking direct proof, they speculated that the trivalent metals might substitute for the (111) top double layer and thus terminate and passivate the surface, but that "... periodically something is also done to relieve the strain ..." and that this something produced the complex LEED pattern. Similarly complicated reflection high-energy electron diffraction (RHEED) patterns were observed much later in 1985 from annealed Si(111) surfaces after Ga (covalent radius 1.26 Å) deposition in the monolayer (ML) range [4] (we define: 1 ML $\widehat{=}$ one atom per substrate surface atom). The reconstruction of Si(111) induced by Cu (metallic bond length 2.56 Å) was also studied early in 1970 by LEED but was first assigned to be commensurate [5]. The Ge(111) (Ge covalent radius 1.23 Å) surface attracted much less attention than Si(111) and corresponding reconstructions, later recognized as being discommensurate, were reported much later. Unusual reconstructions were reported for Ge(111) : In in 1981 [6], Ge(111) : Cu in 1989 [7], and for Ge(111) : Ga in 1992 [8].

The structural properties and peculiarities of all these reconstructions were not recognized immediately since traditional surface analysis tools appeared to be not well suited for their characterization. Two new tools in surface science, scanning tunneling microscopy (STM) [9] and X-ray standing waves (XSW) [10, 11] were invaluable for a thorough understanding. While XSW measurements showed for the case Si(111) : Ga that in the ML (1 ML $= 7.84 \times 10^{14}$ atoms cm^{-2}) range Ga is simply substituting for the Si surface atoms, i.e., the Si atoms of the outermost double layer [12] (cf. Fig. 1), the first STM image revealed a surprising strange surface structure [13, 14]: The surface was tiled by domains, several Si lattice units in size, in a nonperiodic way. The interior of the domains exhibited a hexagonal structure with a lattice constant about 7% larger than

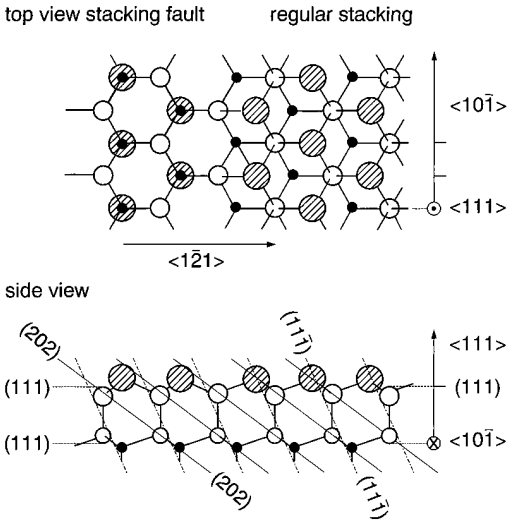

Fig. 1. Substitutional adsorbate on the (111), diamond structure surface in regular stacking sequence as well as with a stacking fault. The (111), (202), and (11$\bar{1}$) diffraction planes are indicated

the 3.84 Å lattice constant of the Si(111) surface. From the XSW results is was clear that the STM was imaging the substitutional Ga atoms. Rehybridization ($sp^3 \rightarrow sp^2 + p_z$, i.e., more graphite like) of the Si–Ga surface layer and inward relaxation of the Ga atoms, as concluded from first principle total energy calculations [12], obviously creates such a forceful stress in the surface that the Si–Ga layer expands and becomes locally, within the domains, incommensurate. The domains are separated by a two-dimensional network of dislocations, i.e., discommensurations.

Quite a number of studies tried to resolve the structure of Si(111) : Cu [15 to 18]. STM images of the Si(111) : Cu surfaces structure were as striking [19 to 21] as the images of Si(111) : Ga. However, despite the wealth of – partially seemingly conflicting – information the microscopic structure of the discommensurate phase of Si(111) : Cu was not understood until XSW results became available [22]. The Cu atoms were found to be adsorbed on the (111) surface in substitutional *and* H_3 sites with considerable downward relaxation. Thus the Si(111) surface bilayer is converted into a densely packed hexagonal layer made of Si and Cu with stoichiometry Cu_2Si. Severe compressive stress again results in local incommensurability and the appearance of domains separated by discommensurations.

Of the discussed class of systems, most thoroughly investigated and fairly well understood up to now are the reconstructions induced by Ga on the Ge(111) surface. At low coverages ($\lesssim 0.1$ ML) Ga stabilizes a superlattice of domains in the interior of which Ge adatoms are in T_4 sites with 2×2 periodicity [23, 24]. The domains are fluctuating in size and are separated by $c(4 \times 2)$ antiphase domain walls [24]. At higher Ga coverage, three different discommensurate phases have been identified in the ML (1 ML= 7.23×10^{14} atoms cm^{-2} on Ge(111)) regime and were studied by LEED, STM, surface X-ray diffraction (SXRD), XSW and ab initio total energy minimization calculations [8, 25 to 28]. One of these three phases, appearing at the highest Ga coverage, is metastable [28] and will not be discussed here. The surface structures of Si(111) : Ga and Ge(111) : Ga are most likely very similar except that a commensurate $\sqrt{3} \times \sqrt{3}\,R30°$ phase with a maximum coverage of 1/3 ML Ga exists on Si(111) [29] but is not stable on Ge(111) [23, 28, 30].

Of the two systems which Lander and Morrison [3] had investigated 1964 with their pioneering LEED work, Si(111) : In has been studied meanwhile by several groups. Quite a number of reconstructions are reported, but, although the atomic structure is not yet

resolved, all the reconstructions seem to be commensurate [31]. The surface phases of Si(111) : Al have not been that intensively studied but it appears that the system behaves analogous to Si(111) : Ga, i.e., there is a commensurate $\sqrt{3} \times \sqrt{3}$ R30° structure at 1/3 ML coverage and the adsorbate becomes discommensurate at higher Al coverage [32].

We wish to clarify the nomenclature we use at this point. The term discommensurate means that the structure is neither commensurate (coherent with the substrate lattice) nor incommensurate (incoherent with the substrate lattice). In fact, discommensurate phases are frequently observed during commensurate–incommensurate (CI) phase transitions (mostly in case of physisorbed systems) driven e.g. by coverage or temperature. Simplified, we can consider the structure of an adsorbate at $T = 0$ as dictated by two competing forces or interaction energies: a) the adsorbate–adsorbate interaction and b) the adsorbate–substrate interaction. If a) is dominant, the adsorbate will be incommensurate, i.e., exhibit its own lattice constant. If b) is dominant, the adsorbate will be commensaturate, i.e., the adsorbate lattice constant will be dictated by the substrate. If a) and b) are competitive, the resulting structure can be discommensurate. This principal behavior was realized already 1938 by Frenkel and Kontorova (FK) [33] and analyzed quite conclusively in the famous paper of Frank and van der Merwe (FvdM) in 1949 [34] (see Fig. 2). Despite extensive simplifications, the behavior of mismatched adsorbate and epitaxial systems was surprisingly well described by the results of the theory. Besides treating the problem in the one-dimensional limit they assumed a harmonic interaction potential between the adsorbate atoms and a sinusoidal interaction potential between substrate and adsorbate. The discommensurate phase consists of domains, in which the adsorbate is close to being in registry with the substrate, i.e., is weakly incommensurate, but strained since it does not exhibit its own lattice constant. The domains are separated by boundaries (discommensurations) where the strain, built up in the domains, is released. In fact, the strain changes sign in these boundaries. If the adsorbate is compressed in the domains, it expands in the domain walls (light walls) and vice versa (heavy walls). It is an important property of such discommensurate structures on semiconductor surfaces that the discommensurations not only passively faciliate strain release but due to the covalent, directional nature of semiconductor bonds the domain walls can adopt different bonding topologies and thus actively influence the total energy of the discommensurate structure. This was first realized for the case Ge(111) : Ga [27, 28]. The stability of the so-called β-phase is largely due to a chemically more passivated bonding situation at the domain boundaries as compared to the γ-phase.

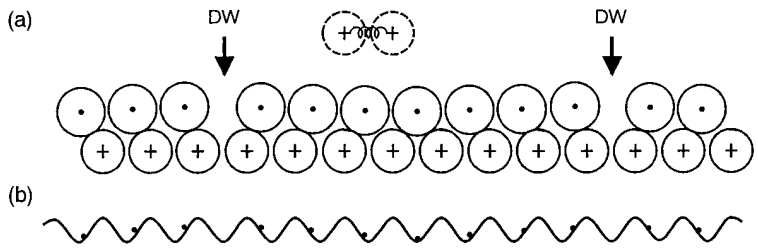

Fig. 2. The Frenkel-Kontorova/Frank-van der Merwe model of a discommensurate adsorbate. Competition between the substrate potential and the adsorbate–adsorbate "spring constant" creates a discommensurate reconstruction. a) Adsorbate on substrate with domain walls (DW). b) Location of adsorbate atoms in the harmonic substrate potential, schematically

In the present report we will review the published results on Si(111) : Ga, Si(111) : Cu, and Ge(111) : Ga, which permits a quite comprehensive description of the structure and properties of the adsorbate induced phases. On the contrary, for Ge(111) : Cu and Ge(111) : In, the experimental findings reported up to now are not sufficient to describe the microscopic structure of these phases. We will report here new XSW results on both systems. For Ge(111) : In we find that (upon annealing) In substitutes for Ge surface atoms at all coverages; however, at higher coverages occupying also partially the substitutional site in the wrong stacking sequence i.e., the surface layer exhibits a h.c.p. instead of f.c.c. stacking sequence with respect to the bulk substrate. For Ge(111) : Cu we find that in case of mild annealing Cu is located in substitutional sites with regular stacking sequence and with a stacking fault. While this (only) disommensurate phase appears on a first view rather similar to Si(111) : Cu our results show that the microscopic structure within the domains exhibits $CuGe_2$ (or possibly CuGe) stoichiometry in contrast to the Cu_2Si stoichiometry within the domains of the Si(111): Cu discommensurate phase. Furthermore, the Ge(111) : Cu discommensurate phase is thermodynamically instable. At higher annealing temperatures ($T \gg 600\,^{\circ}\mathrm{C}$), large amounts of Cu diffuse into the Ge bulk or form 3D islands on the surface leaving most of the Ge(111) surface bare and c(2×8) reconstructed. Unavoidably, the thorough discussion of the rather unusual structural properties of Ge(111) : Cu requires some breadth.

2. XSW Analysis

The new experimental results which will be reported in the following were obtained with the X-ray standing wave technique [11, 35]. An X-ray interference field is generated by Bragg reflecting X-rays by a perfect crystal. The wavefield exists within the overlap region of the incoming and outgoing X-ray beams and resonantly adopts the spacing of the diffraction planes. Within the range of Bragg reflection (i.e., within the resonance) the phase v of the reflected electromagnetic wave changes by π (rad). As a consequence the nodal/antinodal planes of the wavefield are moving inward by half a diffraction plane spacing d_H upon passing the total reflection range from the low angle toward the high angle side of the glancing angle θ.

For hard X-rays, the photoemission probability of core electrons is directly proportional to the X-ray intensity *at the center* of the adsorbing atom. Consequently, if an atom is on the surface of a Bragg reflecting crystal its photoemission or subsequent X-ray fluorescence intensity will exhibit a characteristic dependence on the glancing angle θ indicative for its position z_A with respect to the diffraction planes.

For an XSW measurement we record the photoemission or, as in the following, the fluorescence yield Y_F simultaneously with the reflectively R as a function of the glancing angle θ. The (normalized) yield of a single atom on the surface is given by

$$Y_\mathrm{F} = 1 + R(\theta) + 2\sqrt{R(\theta)}\,\cos\left(v(\theta) - 2\pi z_\mathrm{A}/d_H\right). \tag{1}$$

For a large number of atoms, present within the range of the interference field which is the usual, realistic case, the yield employing a diffraction vector $\mathbf{H}$ can be described as

$$Y_\mathrm{F} = 1 + R(\theta) + 2\sqrt{R(\theta)}\,F^H\,\cos\left(v(\theta) - 2\pi P^H\right), \tag{2}$$

where the two parameters F^H and P^H are called coherent fraction ($0 \leq F^H \leq 1$) and coherent position ($0 \leq P^H < 1$), respectively. Comparison with Eq. (1) shows that for a single atom $F^H = 1$ and $P^H = z_\mathrm{A}/d_H$, i.e., the position of the atom can immediately be determined. On the other hand, if we sample a large number of atoms and the determined yield function exhibits an F^H-value of the order unity, all the atoms must occupy almost the same position with respect to the diffraction planes and this position z_A can directly be inferred from the XSW result P^H. For a wider distribution of positions, F^H will be reduced and P^H will represent an average.

The fluorescence intensity I_F from an adsorbate recorded during an XSW measurement [35] can generally be expressed as

$$I_\mathrm{F} = I_0 Y_\mathrm{F} \tag{3a}$$

$$= I_0 \left[1 + R + 2\sqrt{R}\, D^H \sum_{i=1}^{n} c_i \cos\left(v - 2\pi P_i^H\right) \right] \tag{3b}$$

with Y_F given by Eq. (2). Here P_i^H measures the i-th position z_i^H of the adsorbate with respect to the (hkl) diffraction planes characterized by the diffraction vector $\mathbf{H}$, normalized by the diffraction plane spacing d_H, i.e.,

$$P_i^H = z_i^H H = z_i^H / d_H \,, \tag{4}$$

with $0 \leq z_i^H < d_H$. Furthermore, c_i is the fraction of the adsorbate atoms occupying the i-th position with $\sum c_i = 1$, I_0 is an intensity factor which is proportional to the total number of atoms contributing to the fluorescence, i.e. also proportional to the adsorbate coverage and D^H is the Debye-Waller factor which takes thermal vibrations of the adsorbate into account. The two parameters P^H and F^H are determined by fitting a function given by Eq. (3a) to the measured fluorescence intensity with the fitting parameters I_0, P^H, and F^H.

We can conveniently express F^H and P^H as

$$F^H = \left(G_\mathrm{c}^H + G_\mathrm{s}^H\right)^{1/2} \tag{5}$$

and

$$P^H = (2\pi)^{-1} \tan^{-1}\left(\frac{G_\mathrm{s}^H}{G_\mathrm{c}^H}\right) \begin{cases} +0.5 & \text{if} \quad G_\mathrm{c}^H < 0 \,, \\ +0 & \text{otherwise} \,, \end{cases} \tag{6}$$

where

$$G_\mathrm{c}^H = \sum_{i=1}^{n} c_i \cos\left(2\pi P_i^H\right) \quad \text{and} \quad G_\mathrm{s}^H = \sum_{i=1}^{n} c_i \sin\left(2\pi P_i^H\right). \tag{7}$$

P^H and F^H represent phase and amplitude of the H-th Fourier component of the distribution function of the adsorbed atom from which the X-ray fluorescence is detected.

All XSW measurements reported in the following were carried out at the X15A beamline at the National Synchrotron Light Source at Brookhaven National Laboratory and were performed at room temperature. More details of the XSW technique and the experimental set-up at the X15A are given in [35]. For more details of the XSW analysis we refer to the literature [35, 36, 37].

3. Experimental and Observations

3.1 Ge(111) : Ga

Ga induced phases obtained for $\Theta_{\mathrm{Ga}} \lesssim 0.2$ ML and $\Theta_{\mathrm{Ga}} > 1$ ML are not considered here. These phases, none of which are commensurate, are e.g. described in [24, 25]. STM

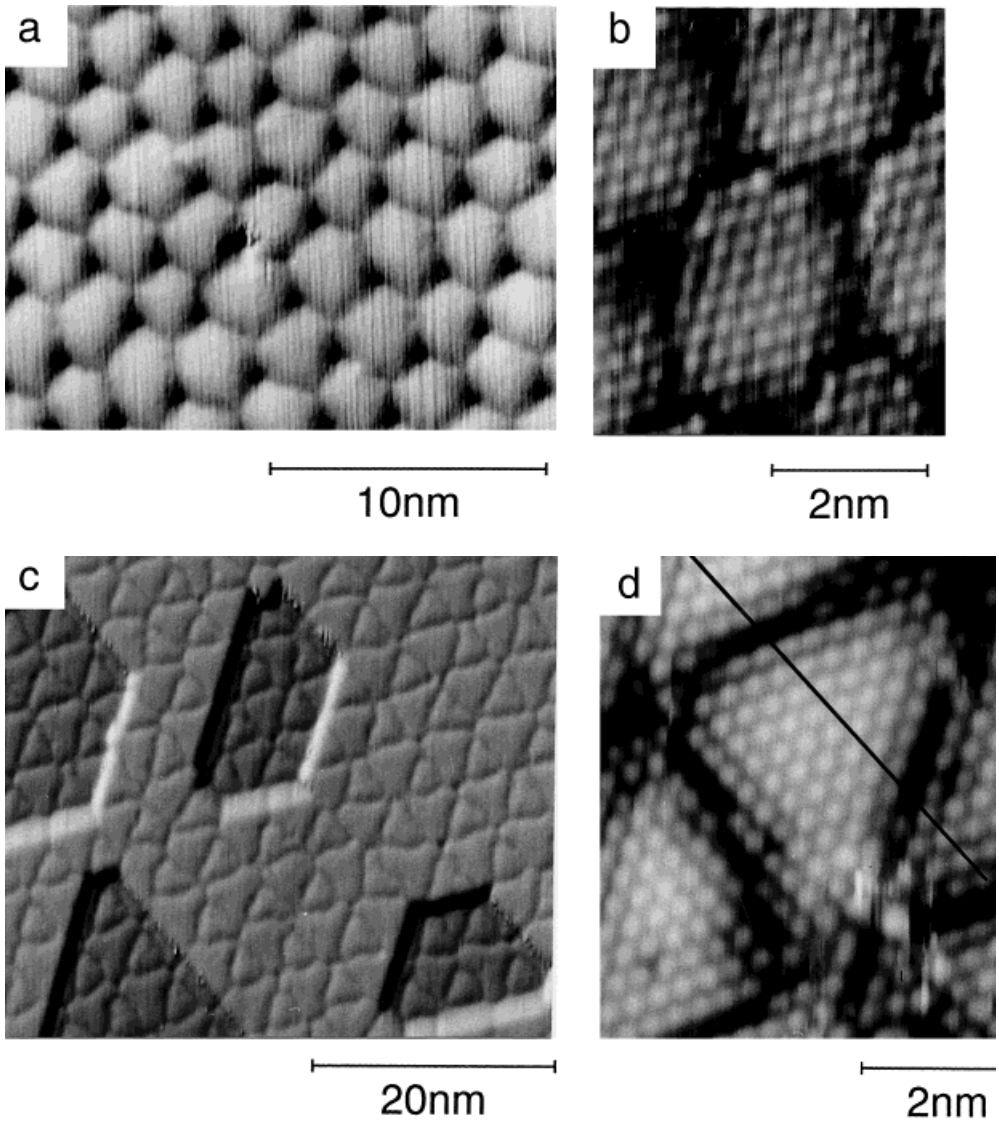

Fig. 3. STM empty states images of the ≈0.7 ML Ga γ-phase (a, b) and β-phase (c, d) of Ge(111) : Ga [27]. The surface is tiled with a nonperiodic superlattice of domains about 7 to 8 and 14 to 16 Ge surface lattice constants ($a_{110} = 4.0$ Å) in size for the γ (a) and β-phase (c), respectively. The interior of the domains (b, d) exhibits a hexagonal lattice with a ≈10% increase in lattice constant compared to $a_{110} = 4.0$ Å. The β-phase exhibits two types of domains in which the stacking sequence with respect to the substrate bulk is different as the line drawn in (d) proves

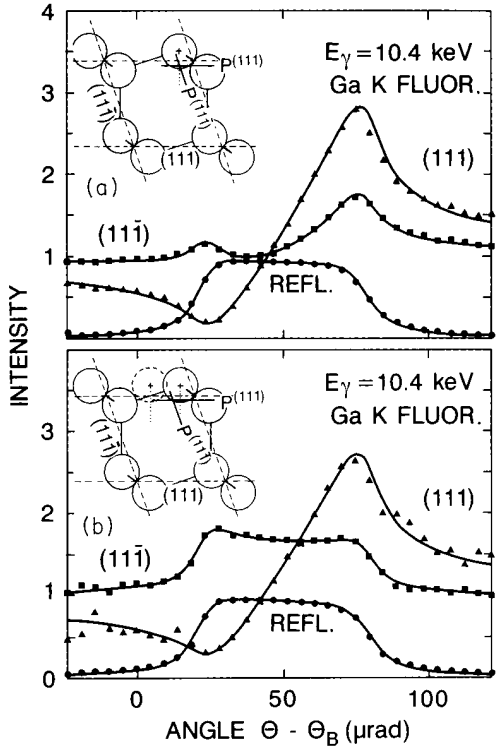

Fig. 4. XSW results for the a) Ge(111):Ga γ-phase and b) β-phase obtained by employing (111) and (11$\bar{1}$) substrate reflection. Shown are reflectivity curves and the Ga-K fluorescence yield. Symbols are experimentally obtained data and lines are fits to the data. With the fits to the fluorescence yield, the structure parameters P^H and F^H are obtained, yielding $P^{111} = 0.95 \pm 0.005$, $F^{111} = 0.95 \pm 0.02$, $P^{11\bar{1}} = 0.83 \pm 0.005$, and $F^{11\bar{1}} = 0.48 \pm 0.01$ for the γ-phase and $P^{111} = 0.95 \pm 0.005$, $F^{111} = 0.87 \pm 0.02$, $P^{11\bar{1}} = 0.74 \pm 0.01$, and $F^{11\bar{1}} = 0.13 \pm 0.01$, for the β-phase. In the insets, the P^{111} and $P^{11\bar{1}}$ results are indicated graphically

images obtained for annealed (≈ 800 K) Ge(111):Ga with Θ_{Ga} in the ML range are shown in Fig. 3. The results of XSW measurements are shown in Fig. 4. Details of the sample preparation and other experimental conditions can be found in [26, 27]. At a saturation coverage of about 0.7 ML Ga, the Ge(111) surface is covered by a nonperiodic superlattice of domains with an average spacing of around $7.4a_{110}$ ($a_{110} = 4.0$ Å for Ge). A phase transition occurs at a coverage above 0.7 ML and at ≈ 0.8 ML the surface is covered with much larger domains (14 to $16a_{110}$) again tiling the surface in a nonperiodic way. For both phases, the γ-phase at 0.7 ML and the β-phase at 0.8 ML, the interior of the domains exhibits a hexagonal lattice with ≈ 4.4 Å lattice constant if empty states are imaged. Filled state images, published in [27], look dramatically different. The interior of the domains appears almost featureless whereas in the case of the γ-phase the domain boundaries are marked by irregular atomic protusions in contrast to the β-phase where the boundaries are also featureless.

For both phases, the (111) XSW results in terms of P^{111} and F^{111} are almost identical. The P^{111} values are indicative of a relaxed substitutional position of the Ga (see Section 1 and 4). However, the $P^{11\bar{1}}$ and $F^{11\bar{1}}$ values for the γ- and β-phases are different. The P^H-values are given in the caption of Fig. 4. For the β-phase, P^{111} and $P^{11\bar{1}}$ do not indicate a high symmetry site. The low $F^{11\bar{1}}$ value for the γ-phase indicates a fairly large in-plane distribution of the Ga around the mean adsorption site. This distribution is even larger for the β-phase as indicated by the even smaller $F^{11\bar{1}}$ value.

3.2 Si(111):Ga

The system Si(111):Ga was studied earlier than Ge(111):Ga, at a time when the nature of the Ga induced phases was much less clear and thus the investigations of Si(111):Ga are less comprehensive except for the commensurate $\sqrt{3} \times \sqrt{3}\,\mathrm{R30}^\circ$ phase [14, 29] which

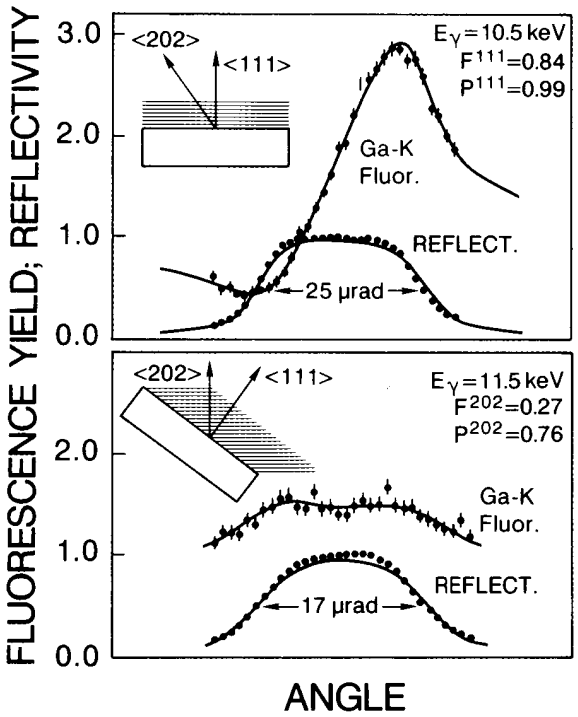

Fig. 5. XSW results for (111) and (202) measurements on Si(111):Ga, ≈ 0.44 ML Ga annealed at 800 K. Shown are the reflectivity and Ga-K fluorescence yield. Symbols are experimental data points and lines are fits to the data. The orientation of the used **H**-vectors and the orientation of the "standing waves" with respect to the sample are schematically indicated

appears at $\Theta_{\mathrm{Ga}} \lesssim 1/3$ ML (on Ge(111) the $\sqrt{3}$ phase is not stable [25, 28]). The results of XSW measurements for a Ga coverage >1/3 ML [30] are shown in Fig. 5. As in the case of Ge(111):Ga (Fig. 4) the (111) measurement probes the distribution of Ga atoms normal to the surface. The (202) measurement, as the $(11\bar{1})$ measurement in Fig. 4, is sensitive to the in-plane registry of the Ga atoms. The results of the measurements shown in Fig. 5 are rather similar to the results in Fig. 4 for the β-phase for Ge(111):Ga. The Ga atoms are located within the surface layer in relaxed substitutional positons. The P^H values obtained by fits to the fluorescence yield curves in Fig. 5 are shown in Fig. 6. Laterally, the adsorption site(s) and the Ga distribution around these sites for this Si(111):Ga preparation mut be very similar to those for the Ge(111):Ga β-phase.

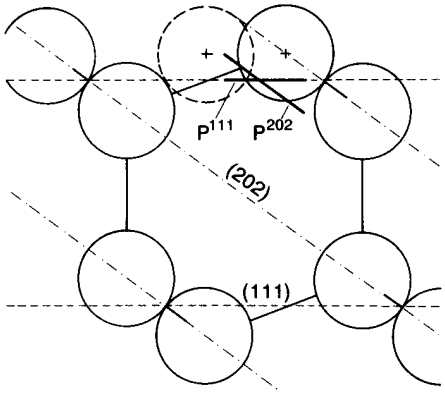

Fig. 6. Graphical representation of the P^H values obtained by the fitted fluorescence yield curves in Fig. 5. The P^{111} and P^{202} values are plotted in a sideview of the Si(111) surface

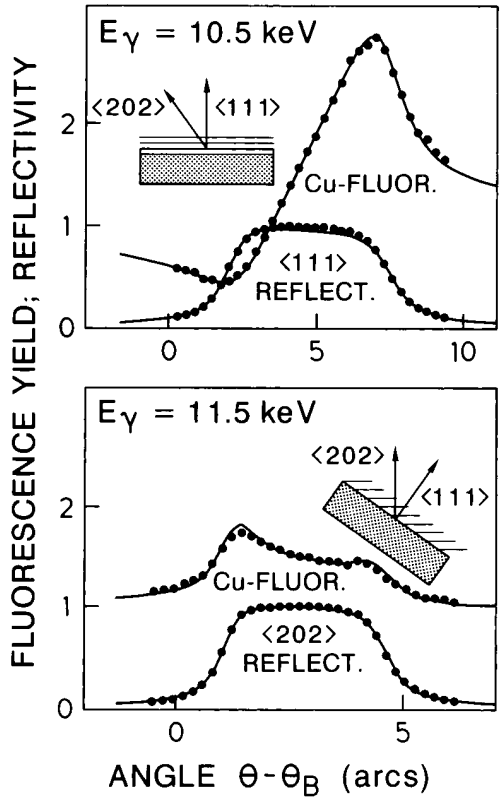

Fig. 7. XSW results for Si(111):Cu, 1.3 ML annealed at 950 K. Shown are the results for a (111) and a (202) measurement. Symbols are experimental data, lines are fits to the data. The geometry for the (111) and the (tilted) (202) measurements is indicated in the figure. The fits yielded $P^{111} = 0.99$, $F^{111} = 0.81$, $P^{202} = 0.70$, $F^{202} = 0.27$

3.3 Si(111):Cu

Only one Cu induced structure is observed on the Si(111) surface which forms for annealing temperatures above 800 K. STM images of this pseudo 5×5 structure, usually denoted as Si(111):Cu-'5×5' are reported by Wilson and Chiang [19], Demuth et al. [20] and Mortensen [21]. As for the previously shown cases of Ga induced structures, the reconstruction is not periodic. The average periodicity of the hexagonal domain superlattice is 5.6×5.6 [22]. For comparison we reproduce [22] in Fig. 7 the results of (111) and (202) XSW measurements for Cu on Si(111), annealed to 950 K. Coverages in the range 0.3 to 3 ML were investigated by XSW and a saturation coverage of 1.3 ML was established. As for the two previously discussed cases Ge(111):Ga and Si(111):Ga, the P^{111} value is indicative of a Cu position within the Si(111) surface diffraction plane. (The position of the (111) surface diffraction plane is given by $P^{111} = 0.0 \bmod n$.) But note that $F^{111} = 0.81$, a value which could not be increased despite careful preparation, indicates some distribution around the average position $P^{111} = 0.99$. Again the F^{202} value, which is sensitive to the in-plane registry of the Cu atoms, is rather small indicating that the Cu shows a fairly large distribution around the mean adsorption site within the surface plane. This mean Cu position, given by the intersection of P^{111} and P^{202} (Fig. 8), is similar to the one obtained for the Ge(111):Ga β-phase (Fig. 4). However, note that the Cu saturation coverage with 1.3 ML is significantly larger than 1 ML.

3.4 Ge(111):Cu

STM images of the Cu deposited Ge(111) surface are shown in Fig. 9. Covered with ML amounts and after a mild annealing to 400 to 500 K, a superlattice of domains is observed on the surface (cf. Fig. 9a, b). The lattice exhibits hexagonal symmetry with a spacing of the domains of about $9a^{\mathrm{Ge}}_{110}$. The domains are aligned along the family of the substrate surface $\langle 101 \rangle$ directions. The surface structure seems rather similar to Si(111):Cu-'5×5'. At RT it is not possible to resolve the structure of the interior of the

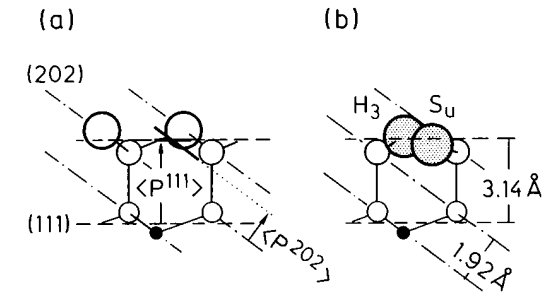

Fig. 8. a) Graphical representation of the XSW results in terms of P^{111} and P^{202}, plotted in a sideview of the (111) surface. b) The two adsorption sites of Cu on Si(111). c), d) Si(111) surface in c) topview and d) sideview. Right-hand part of the surface with Cu (shaded) in substitutional (S_u substitutional in upper part of bilayer) and H_3 sites simplifyingly shown in commensurate arrangement

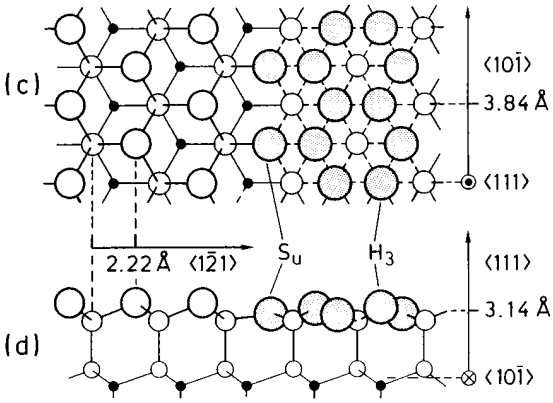

domains with STM. However, atomic resolution is obtained at 50 K as shown in Fig. 9d, e. A hexagonal arrangement of protrusions, spaced at 4.2 Å, can be distinguished in the interior of the domains. At positive sample bias (emtpy state images) the domain boundaries appear as depressions (for filled state images we refer to [38]).

Annealing to above 500 K leads to the reappearance of areas of clean Ge(111) reconstructed c(2 × 8) (cf. Fig. 9c). In comparison with the well known c(2 × 8) reconstruction the crystallographic orientation of the domain superlattive, as noted in Fig. 9b, c, d, f, can now be determined. For higher coverage and moderate annealing temperature, hexagonal shaped, three-dimensional (3D) clusters appear on the surface (cf. Fig. 9f). For sufficiently high annealing temperature ($T > 750$ K), the discommensurate phase disappears completely and the surface is covered by the 3D islands and c(2 × 8) reconstructed areas.

The results of (111) and (11$\bar{1}$) XSW measurements for 1 ML Cu annealed to 500 K are shown in Fig. 10. The fluorescence yield curves look strikingly similar to the ones obtained for Si(111):Cu (cf. Fig. 7), thus indicating again a basically substitutional adsorption site for the Cu. In Fig. 11 the P^{111} and $P^{11\bar{1}}$ values are plotted again in a sideview. The intersection marks a similar mean position as in the case of Si(111):Cu. However, several measurements confirmed that the (111) "substitutional coverage", i.e., the product of F^{111} and Θ_{Cu}, never exceeded 0.7 ML in contrast to Si(111):Cu where $F^{111}\Theta_{Cu}$ reached 1.1 ML.

The annealing behavior of Ge(111):Cu (1.5 ML) studied with XSW is shown in Fig. 10c, d. Annealed to 700 K, the fit of the fluorescence yield using the function

$$Y_F = I_0^{-1}[1 + R + 2\sqrt{R}\,F^{111}\cos(v - 2\pi P^{111})]\,, \tag{8}$$

which describes the yield expected from *any surface adsorbate system*, starts to give a poor result and F^{111} is strongly reduced. Upon annealing to 800 K the shape of the fluorescence yield curve changes strongly and trying to fit a function given by Eq. (8) to

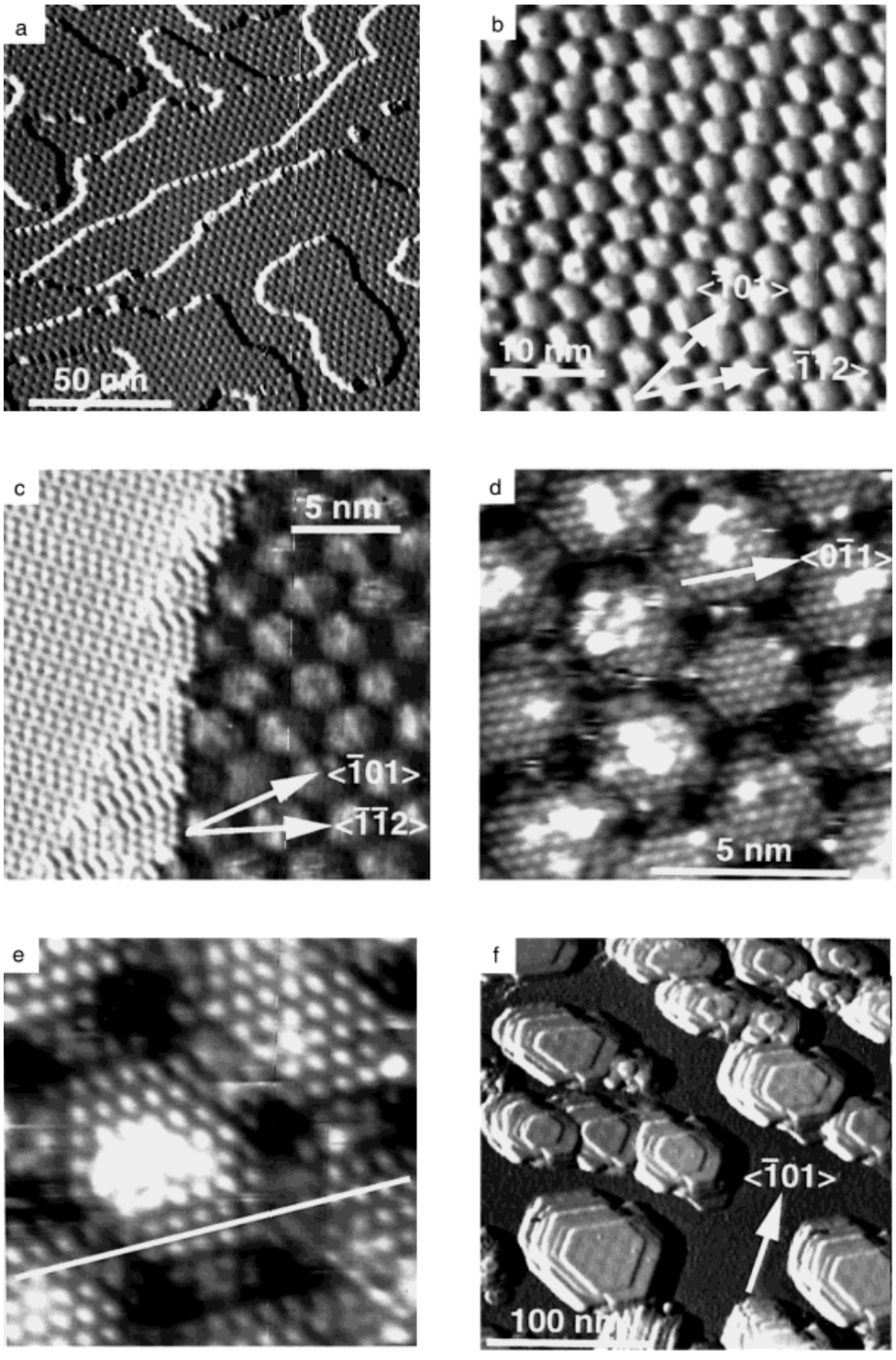
a
50 nm
b
<$\bar{1}$01>
10 nm
<$\bar{1}$$\bar{1}$2>
c
5 nm
<$\bar{1}$01>
<$\bar{1}$$\bar{1}$2>
d
<0$\bar{1}$1>
5 nm
e
f
<$\bar{1}$01>
100 nm

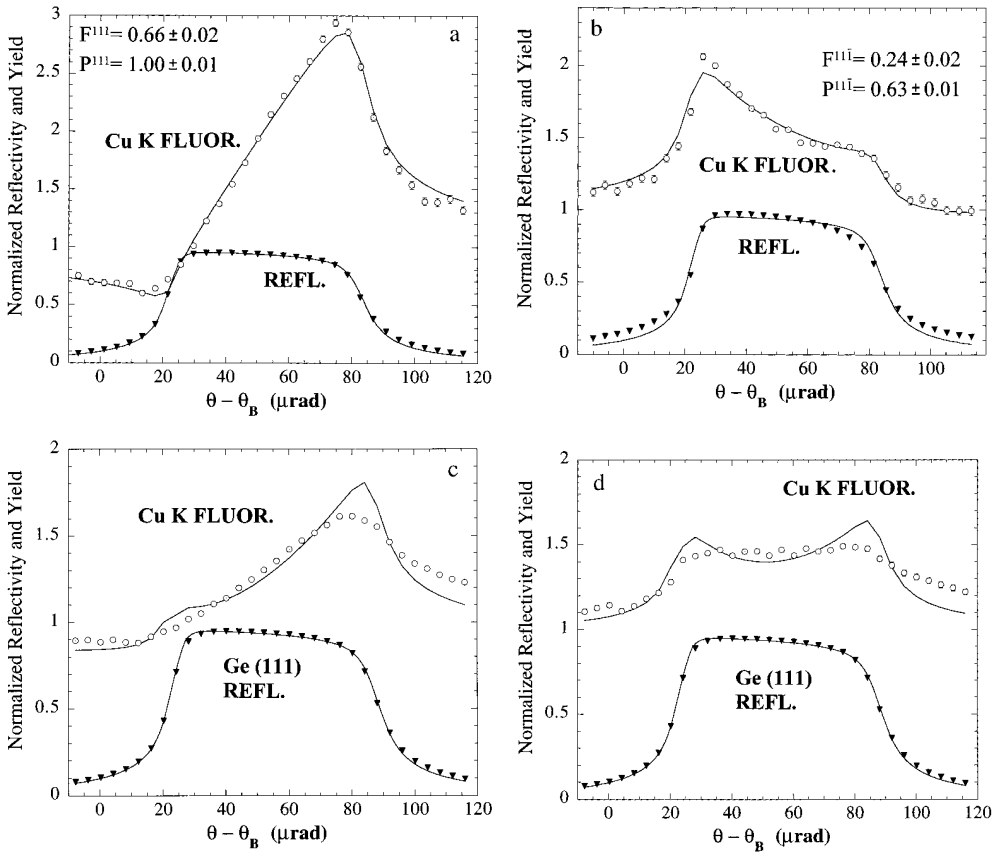

Fig. 10. XSW results for Ge(111) : Cu. a), b) 1 ML annealed at 500 K, a) (111) measurement, b) (11$\bar{1}$) measurement; c), d) 1.5 ML Cu d) annealed at 700 K, d) annealed at 850 K

the yield gives a very poor result. In Fig. 12, P^{111} and F^{111} are plotted for 1.5 ML on Ge(111) as a function of annealing temperature.

3.5 Ge(111):In

In Fig. 13 STM images of the annealed Ge(111):In surface are shown for increasing In coverages and different resolutions. At coverages below 0.3 ML, darker stripes of constant

◀

Fig. 9. Empty state STM images of the annealed Ge(111) : Cu surface [38]. a) Overview, 2 ML Cu annealed at ≈400 K, showing the domain superlattice introduced by Cu. Image obtained at room temperature. b) As a) but showing the reconstruction on a small scale. c) High resolution STM image of the discommensurate phase (right-hand side) in coexistence with the Ge(111)-c(2×8) reconstruction (left-hand side). d) High resolution STM image obtained at 50 K showing the internal lattice of the domains. e) A closeup of the domains. The line indicates a different stacking sequence of the Cu with respect to the Ge substrate in adjacent domains. Image obtained at 50 K. f) Images of Ge(111) : Cu with 4 ML Cu annealed at ≈500 K. Part of the Cu starts to cluster in epitaxial islands made of Cu or Cu germanide

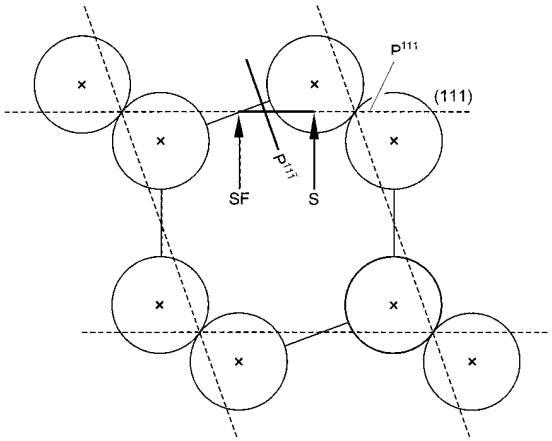

Fig. 11. Schematic representation of the P^{111} and $P^{11\bar{1}}$ values for the measurements on Ge(111) : Cu shown in Fig. 10a, b. The arrows indicate the lateral positions for the substitutional (S) and faulted substitutional (SF) sites

width are separated by brighter stripes of varying width where individual atomic protrusions can be distinguished. They correspond to Ge adatoms in T_4 sites in a local 2×2 arrangement [39]. The In is located in the dark stripes. The width of the white adatom stripes on average *decreases* with *increasing* In coverage until for the maximum In coverage for the striped phase the white stripes consist only of a zig-zag chain of Ge adatoms. Higher resolution STM images (cf. Fig. 13b) show also atomic protrusions within the dark stripes. However, it is not clear whether Ge or In atoms are imaged.

At coverages >0.3 ML new phases appear on the surface [6]. Characteristically, they all consist of a superlattice of domains, with seemingly hexagonal symmetry [39] (cf. Fig. 13c). At higher coverage, the striped phase disappears. Within the "hexagonal phases" atomic protrusions can be distinguished within the domains which exhibit locally also hexagonal symmetry (cf. Fig. 13d). The lattice constant within the domains is strongly increased ($>10\%$) compared to the Ge(111) constant of 4.0 Å [39].

The results of (111) and (11$\bar{1}$) XSW measurements, obtained with an X-ray energy of $E_\gamma = 6.15$ keV, are shown in Fig. 14 and 15. The signature of the In L fluorescence yield as a function of angle clearly reveals again the substitutional adsorption site for the In in the striped phase of Ge(111):In. Different from the results of all other systems presented here so far, the coherent fraction for the "tilted" measurement, the (11$\bar{1}$) scan,

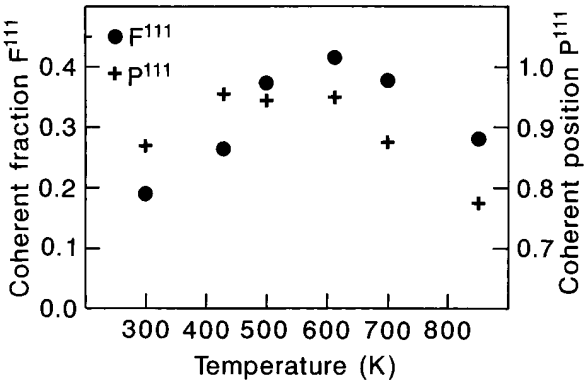

Fig. 12. XSW F^{111} and P^{111} values for 1.5 ML Cu on Ge(111) plotted as a function of annealing temperature. The error bars are typically smaller than the size of the symbols

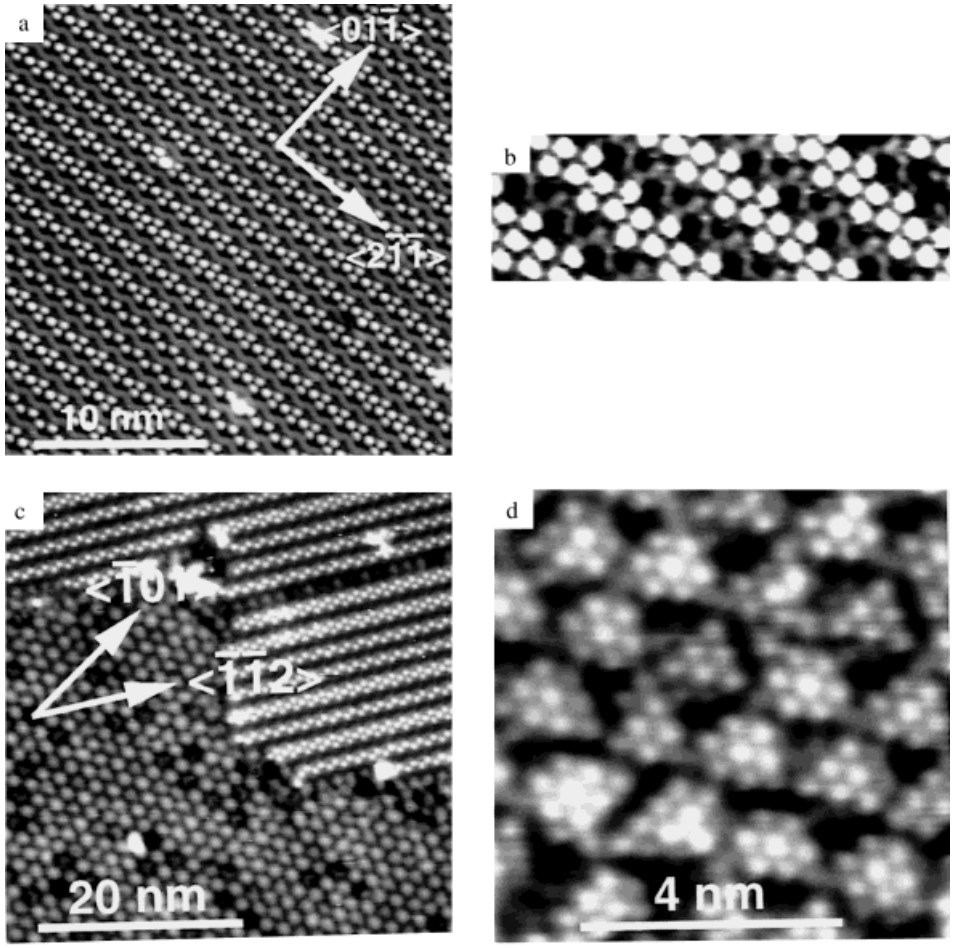

Fig. 13. STM empty state images [39] of annealed Ge(111) : In. a) The "striped phase" at 0.25 ML In overage. b) High resolution (40×125 Å) image of the striped phase. c) 0.3 ML In at the phase transitions from the striped phase to the hexagonal reconstructions. d) High resolution image of the hexagonal domain superstructure, $\theta_{\mathrm{In}} = 0.9$ ML

which is sensitive to the in-plane In distribution, shows also a comparably high coherent fraction of $F^{11\bar{1}} = 0.66$ (Fig.14b). The results obtained for one of the higher coverage, hexagonal phases are shown in Fig. 14c and d. For this preparation, LEED revealed a characteristic $4\sqrt{3} \times 4\sqrt{3}\,\mathrm{R}30^\circ$ diffraction pattern [6, 39], i.e., this reconstruction is periodic (or higher-order commensurate). Again, the (111) results carries the signature of the substitutional In position; however, note that the coherent position shows a slightly lower value ($P^{111} = 0.96$) than for the striped phase ($P^{111} = 0.99$). Also, the coherent fraction is somewhat reduced from $F^{111} = 0.90$ for the striped phase to $F^{111} = 0.74$. However, the $(11\bar{1})$ coherent fraction has decreased strongly ($F^{11\bar{1}} = 0.29$) and the $P^{11\bar{1}}$ value also changed significantly by $\Delta P^{111} = 0.09$ which can be distinguished already by the difference in the shape of the fluorescence yield curves in Figs. 14b and d.

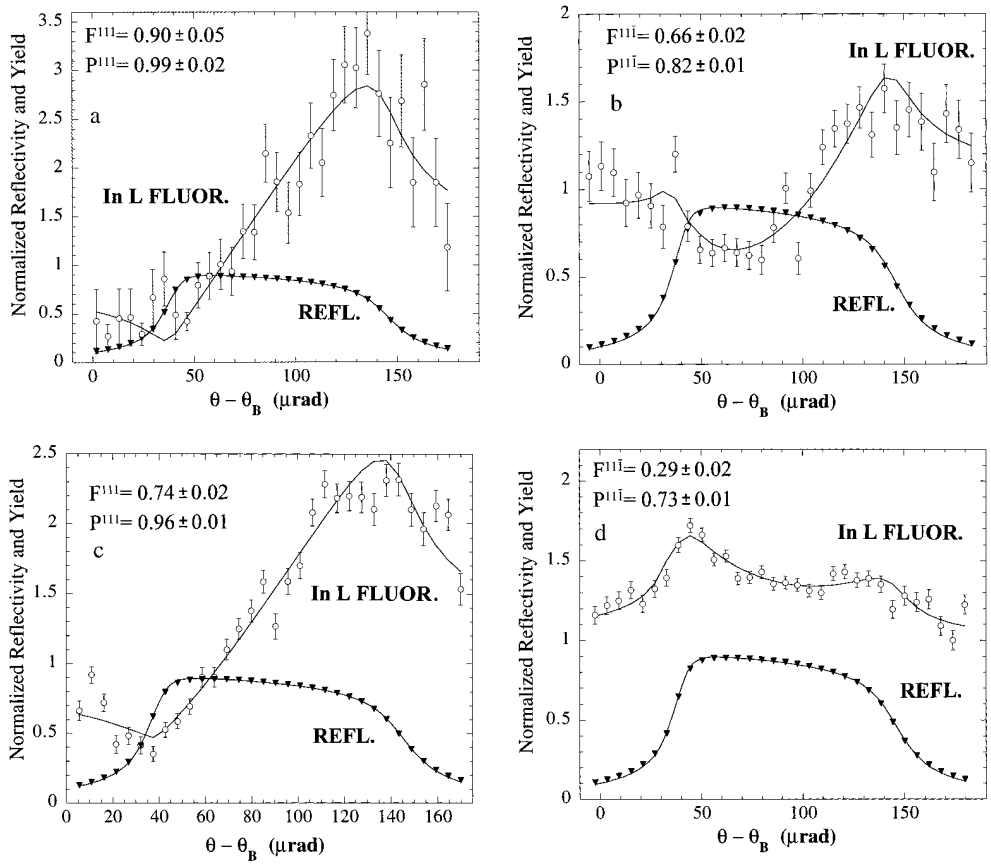

Fig. 14. Results of XSW measurements on annealed Ge(111) : In. Symbols are experimental data; lines are fitted curves. a), b) Striped phase, ≈0.25 ML In, (111) and (11$\bar{1}$) measurements, respectively, c), d) hexagonal phase, ≈0.9 ML In, (111) and (11$\bar{1}$) measurements, respectively

4. Discussion

Before we discuss the individual reconstructions we will point out some general features of these adsorbate systems. The (111) XSW coherent positions are, with rather small variations, the same for all these metal atoms in the contemplated reconstructions. All coherent positions are close to $P^{111} = 0.0$. A substitutional position in the surface layer, i.e., within the top part of the surface double layer of an ideally terminated (111) surface would correspond to $P^{111} = 0.125$; a position which is located $0.125 d_{111}$ above the (111) surface diffraction plane (cf. Fig. 1). This means that all the considered metal adsorbate atoms have relaxed inward by $\gtrsim 0.125 d_{111}$, i.e., by 0.3 to 0.4 Å. For the trivalent atoms, a substitutional position (i.e., P^{111} of about 0.125) in the (111) surface seems natural since all their three valence electrons can saturate the valence orbitals of the underlying Si or Ge and the surface would be depleted of dangling bonds. However, a position close to $P^{111} = 0.125$ would only be possible if the metal atoms adopt a sp^3 hybridization with the characteristic tetrahedral bonds. This is obviously not the case.

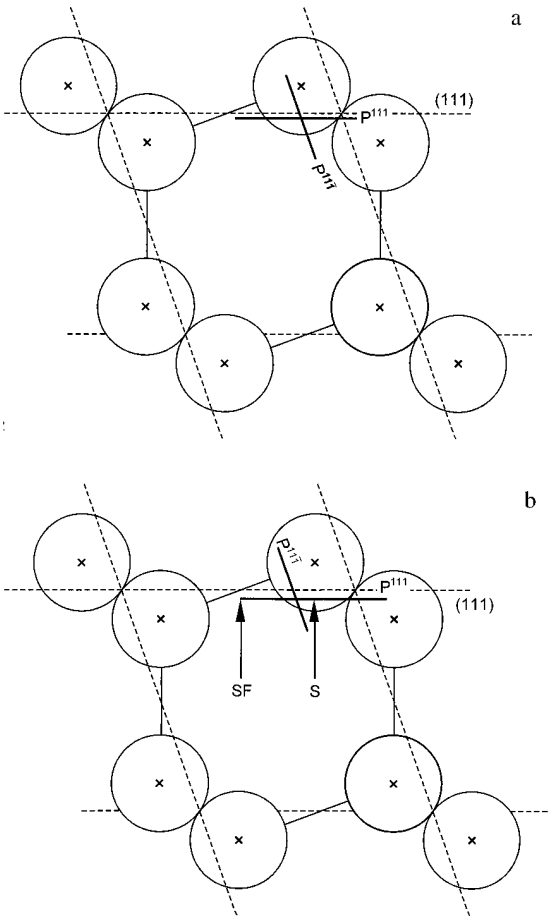

Fig. 15. a) P^{111} and $P^{11\bar{1}}$ for the striped phase from Fig. 14a, b in a graphic representation. b) P^{111} and $P^{11\bar{1}}$ for the hexagonal phase from Fig. 14c, d in a graphic representation. The arrows indicate the lateral positions for the substitutional (S) and faulted substitutional (SF) sites

Total energy calculations for this kind of substitution for Ge(111):Ga and Si(111):Ga [14, 26, 30] have shown that the hybridization of the surface layer is more like $sp^2 + p_z$, i.e., similar to graphite. The (111) double layer becomes rather planar with a correspondingly lowered position of the metal atoms. Since the covalent radii of Ga (2.52 Å), Cu (2.56 Å), and In (2.88 Å) are all considerably larger than the covalent radii of Ge (2.45 Å) and Si (2.35 Å), a tremendous stress must be generated in the surface layer by the inward relaxation. We should mention here that this scenario is well established for Ga and rather likely for In, but, while it is clear from the XSW results that Cu substitutes in a strongly inwardly relaxed substitutional position, the nature of the chemical bond of Cu and its hybridization is as yet not clear. We will discuss this in more detail below.

The substitution by metal atoms could basically lead to a chemically passivated 1×1 surface structure but the consequently produced violent compressive stress prohibits this for all discussed cases. This is proven by those XSW measurements which are sensitive to the in-plane structure which are the $(11\bar{1})$ and (202) scans in the present cases.

4.1 Ge(111):Ga

In the γ-phase (cf. Figs. 3a, b and 4a) the Ga atoms are substituting for the Ge surface atoms basically as shown in the right-hand part of Fig. 1. As the experimental value ($P^{111} = 0.95 \pm 0.005$) shows, the Ga atoms are relaxed inward by $\Delta P^{111} d_{111}^{\mathrm{Ge}} = 0.175$ (± 0.005) $d_{111}^{\mathrm{Ge}} = (0.57 \pm 0.02)$ Å with respect to the bulk-like, unrelaxed Ge surface layer. The high (111) coherent fraction $F^{111} = 0.95$ shows that all Ga atoms are located in a single layer with an insignificant height distribution normal to the surface. However, the relatively small value of $F^{11\bar{1}} = 0.48$ indicates a significant lateral distribution of Ga

positions, centered around the mean position which is the relaxated substitutional site as proven by $P^{11\bar{1}} = 0.83 \pm 0.005$. For a value of $P^{111} = 0.95$, the calculated value for the relaxed substitutional position would be $P^{11\bar{1}}_{\mathrm{S,calc}} = 0.82$ in good agreement with the experimentally observed value. The microscopic structure of the Ge(111) : Ga surface was additionally confirmed by adsorbing Ga on a double layer of Ge on Si(111) [40, 41]. With this trick, XSW measurements confirmed that the surface layer consists of an almost flat GeGa bilayer with Ga occupying the upper and Ge the lower half.

STM images with atomic resolution of the interior of the domains of the γ-phase [27], as shown in Fig. 3b, reveal the hexagonal arrangement of the substitutional Ga atoms but with a lattice constant increased by about 10% compared to the substrate lattice.

The physical picture of the internal structure of the domains of the γ-phase is as follows: within the center of each domain, the surface atoms are laterally practically in registry with the substrate bulk. With increasing distance from the center of the domains, the Ga surface atoms are progressively more and more out of registry. This is schematically shown in Fig. 16 for an idealized, hexagonally shaped domain. A representative $(11\bar{1})$ diffraction plane in the center of the domain is indicated. Relative to the $(11\bar{1})$ diffraction *plane*, the individual Ga layers indexed by i change their $P_i^{11\bar{1}}$ values determined by the mismatch ε and their distance from the center plane. The summation of Eq. (7) can be written down as

$$G^{11\bar{1}}_{\mathrm{c,s}} = \sum_{i=-4}^{+4} c_i \begin{matrix}\sin\\ \cos\end{matrix} [2\pi(P^{11\bar{1}}_{\mathrm{S}} + i\varepsilon)] \tag{9}$$

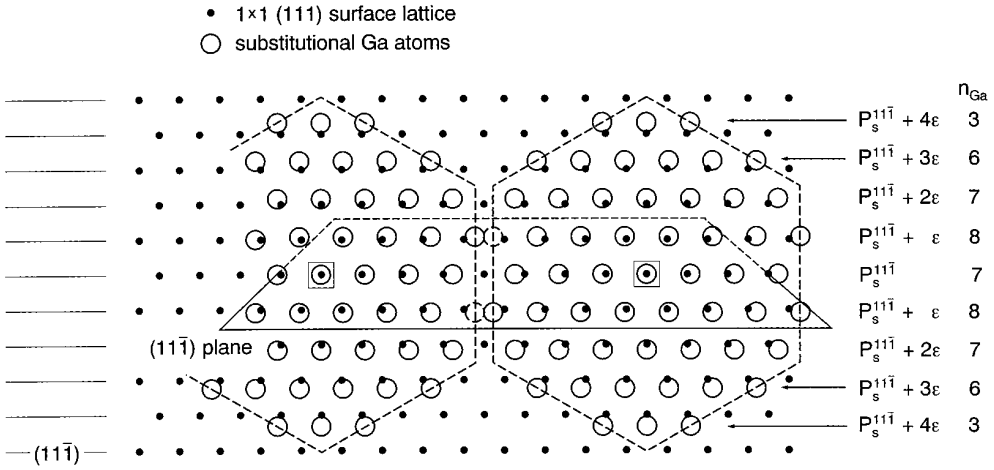

Fig. 16. Schematic model of the microscopic structure of the γ-phase of Ge(111) : Ga. Ga substitutes for the Ge surface atoms leading to a surface layer with GeGa stoichiometry with a mismatch of ≈8%. Only the Ga atoms are shown. The surface strain leads to the appearance of domains. The marked center of the domains is at a symmetric lattice position with respect to the ideal 1×1 lattice which is indicated. The domain boundaries are depleted of Ga. The two shown domains exhibit a size of 8×8. However, the γ-phase displays a nonperiodic superstructure and the size of the domains is fluctuating between 7×7 and 8×8 with an average of 7.4×7.4 [25]. A $(11\bar{1})$ diffraction plane passing through the center of the domains is shown representative of the whole family of parallel diffraction planes indicated by the lines

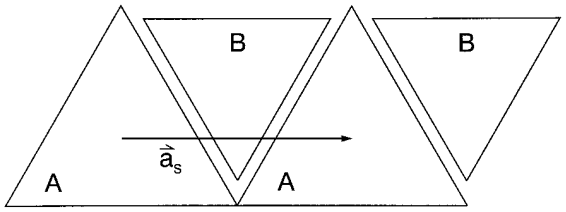

Fig. 17. Schematic model of the domain superstructure of the Ge(111) : Ga β-phase. For the β-phase, the length of the superlattice unit cell $|\mathbf{a}_S|$ varies between 14 and 16 times $a_{110}^{Ge} = 4.0$ Å

with the mismatch ε, the commensurate substitutional Ga adsorption site $P_S^{11\bar{1}} = 0.83$ (= site in the center of the domain), and $c_i = n_{Ga}/55$ where 55 is the total number of Ga atoms within one domain and n_{Ga} is listed in Fig. 16. With $\varepsilon = 0.08$, i.e., a mismatch of 8% in the interior of the domains we obtain $F^{11\bar{1}} = 0.49$. This value is in accordance with the experimentally observed $F^{11\bar{1}} = 0.48$. The resultant coherent position is unaffected by the mismatch in the interior of the domains, i.e. $P^{11\bar{1}} = P_S^{11\bar{1}} = 0.83$. From the results of surface X-ray diffraction measurements [25] a mismatch of 7.5%, i.e, $\varepsilon = 0.075$, was deduced, which is in good agreement with the above determined value.

The β-phase exhibits two different types of domains, A and B (cf. Fig. 3c, d), schematically reproduced in Fig. 17. The superstructure represents a reconstruction of much larger scale than the lattice of the γ-phase. It is also not periodic: the size of the lattice constant fluctuates roughly between 14 and 16 times a_{110}^{Ge} with an average of about 60 Å ($= 15a_{110}^{Ge}$). There is a difference in size between domains A and B and the stacking sequence of the surface (Ga) atoms is different in both domains [27]. I.e., in the larger domains the Ga atoms are located in a substitutional adsorption site. In the smaller domains (B) the Ga atoms are located in a substitutional position but with a stacking fault in the surface layer (cf. Fig. 1). The interior lattice of the domains is strained by about 7 to 8% as in the γ-phase but the stacking fault permits a chemically passivated bonding situation within the domain walls [27, 28]. I.e., in contrast to the domain walls of the γ-phase, there are practically no dangling bonds present within the domains walls of the β-phase. The strain pattern within the domains is obviously not isotropic (which seems to be the case at least approximately within the domains of the γ-phase). STM images show wavy atomic rows within the domains [27].

The larger number of more than 150 Ga atoms contained in the two domains A and B renders the construction of a realistic, microscopic model from which $F^{11\bar{1}}$ and $P^{11\bar{1}}$ values could be calculated extremely difficult. A calculation similar to the one performed above for the γ-phase, assuming now two mean positions, a domain size as determined by the STM measurements and an *isotropic* strain distribution does not give a good agreement between observed and calculated $F^{11\bar{1}}$ and $P^{11\bar{1}}$ values.

If we assume 60% of the Ga atoms in domain type A ($P_S^{111} = 0.83$ without stacking fault) and 40% in domain type B ($P_{SF}^{11\bar{1}} = 0.50$, with stacking fault), all of them with zero mismatch, $F_{ZM}^{11\bar{1}} = 0.54$ and $P_{ZM}^{11\bar{1}} = 0.72$ is calculated. The 60/40 ratio reflects the observed ratio of the domain sizes for the type A and B. For a ratio of 65/35 we can calculate $F^{11\bar{1}} = 0.57$ and $P^{11\bar{1}} = 0.74$ which would reproduce exactly the experimentally observed $P^{11\bar{1}}$ value. The experimentally observed coherent fractions are much smaller because the mismatch (strain) in the overlayer leads to a distribution of positions around these two mean values $P_S^{11\bar{1}} = 0.83$ and $P_{SF}^{11\bar{1}} = 0.50$. Because of the large number of atoms contributing, we will now approximate the distribution of atoms around the mean positions by a Gaussian profile characterized by a standard deviation $\delta P^{11\bar{1}}$. The

experimentally observed coherent fraction $F_{\mathrm{exp}}^{11\bar{1}} = 0.13$ is then determined by two factors

$$F_{\mathrm{exp}}^{11\bar{1}} = f_{\mathrm{G}} F_{\mathrm{ZM}}^{11\bar{1}} \tag{10}$$

with

$$f_{\mathrm{G}} = \exp - [2\pi^2 (\delta P^{11\bar{1}})^2] \tag{11}$$

being the $(11\bar{1})$ Fourier coefficient of the Gaussian distribution function which can also be viewed as static Debye-Waller factor. With $F_{\mathrm{exp}}^{11\bar{1}} = 0.13$ and $F_{\mathrm{ZM}}^{11\bar{1}} = 0.54$ we obtain $f_{\mathrm{G}}^{11\bar{1}} = 0.24$ and thus $\delta P^{11\bar{1}} = 0.27$, i.e., a standard deviation of 0.83 Å for the distribution of positions around the mean position in the $\langle 11\bar{1} \rangle$ direction surface plane which corresponds to a 0.88 Å standard deviation laterally. If we perform a similar calculation for the γ-phase, assuming a Gaussian distribution profile around the mean position, we obtain $\delta P^{11\bar{1}} = 0.19$. This means that the strain is similar in the γ- and β-phases. The larger width of the position distribution profile in the β-phase is mostly determined by the larger domain size.

4.2 Si(111) : Ga

As we stressed earlier [30] the system Si(111) : Ga behaves similarly to Ge(111) : Ga. However, the STM and XSW data available for Si(111) : Ga are much less comprehensive. Reported STM measurements [13] as well as XSW measurements (cf. Fig. 5 and [30]) were most likely performed on not very well ordered surfaces covered with a mixture of the Si(111) : Ga γ- and β-phases. In particular for XSW measurements, the preparation of a single, well defined surface phase is very important for the evaluation of the observed F- and P-values since we record the X-ray fluorescence from the *whole entity* of a particular kind of atom in whatever phase they cover the surface and whether they are ordered or not (i.e, we are measuring the absolute value of the **H** Fourier component). Nevertheless, the determined P^{111} value for Si(111) : Ga shows clearly that Ga is substituting for Si in the top surface layer [12]. The $P^{11\bar{1}}$ value demonstrates that this is not only happening in the regular stacking sequence but also with a stacking fault at the surface. For regular stacking exclusively (pure γ-phase), $P^{202} = 0.82$ is expected from $P^{111} = 0.99$. The experimental value of $P^{202} = 0.76$ indicates that about 10 to 20% of the surface may be covered with the β-phase. The low value $F^{202} = 0.27$ documents a fairly wide lateral distribution around the mean adsorption sites.

Otsuka and Ichikawa [4] had reported RHEED observations of a 6.3×6.3 and a 11×11 reconstruction on annealed Si(111) surfaces for Ga coverages in the ML range. Later STM observations confirmed the 6.3×6.3 structure and showed that 6.3×6.3 reflects the symmetry and average periodicity of the discommensurate domain superlattice [12]. Recently it became clear that the 6.3×6.3 and the 11×11 phases are the equivalent of the γ- and β-phase, respectively, of Ge(111) : Ga [30]. Since the Si lattice is 4% smaller than the Ge lattice, the substitutional Ga produces a higher stress in the Si(111) surface and consequently the surface layer exhibits a larger mismatch compared to Ge(111) which results in smaller domain sizes. With 7% the early STM study has underestimated the mismatch [13].

4.3 Si(111) : Cu-'5 × 5'

Since the Cu saturation coverage of the Si(111) : Cu-'5×5' reconstruction is clearly larger than 1 ML, the surface structure cannot be explained by Cu substitution in the sur-

face layer alone. For a commensurate Ge(111) : Cu structure this would give a coverage of 1 ML. For a discommensurate structure as a result of a SiCu layer with an increased surface lattice constant, the saturation coverage would be expected to be less than 1 ML. The model for the microscopic structure is shown in Fig. 8b and exhibits two Cu atoms per 1×1 unit cell in the commensurate limit. Cu is in the substitutional position (S_u) at $P_S^{111} = 0.89$ *and* in the hollow, threefold coordinated H_3 site at $P_{H_3}^{111} = 0.06$, i.e. 0.34 Å below and 0.19 Å above the surface diffraction plane (cf. Fig. 1), respectively. Thus, because there are two Cu atoms per 1×1 surface unit cell, the stoichiometry is basically Cu_2Si. However, just as the Ga in the previously discussed cases, the Cu in the surface layer generates tremendous stress and the surface lattice constant expands by 10%, generating a network of discommensurations and a non-commensurate superstructure of domains with an average periodicity of 5.6×5.6. Because of the compressive (positive) strain ($\varepsilon = 0.1$) within the domains, the discommensurations represent light walls, i.e., they are depleted of Cu. Electron diffraction [18] and X-ray diffraction measurements showed that the interior lattice of the domains is rotated by 3° with respect to the substrate crystallographic directions.[2]) With the above given two positions of the Cu, the 10% mismatch, the 3° rotation, light walls and the observed domain size, P^H and F^H values which are calculated using Eqs. (5) to (7) are in good agreement with the experimental observed values. The Si(111) : Cu-'5×5' structure and its XSW analysis are described in more detail in [22] and [35].

4.4 Ge(111) : Cu

Judging from the overall appearance of the domain superlattice in the STM images (cf. Fig. 9a, b and [21]) and the mean adsorption position as determined by XSW (cf. Fig. 8a and Fig. 11) the Si(111) : Cu-'5×5' and the Ge(111) : Cu superstructure seem, except for the domain sizes, at first glance very similar. However, closer inspection reveals that this first impression is misleading; there are rather pronounced differences:

a) The saturation coverage for the discommensurate Ge(111) : Cu phase is less than 1 ML in contrast to 1.3 ML for Si(111) : Cu-'5×5'.

b) The discommensurate Ge(111) : Cu phase exhibits a rather low formation temperature of about 400 K in contrast to a formation temperature of about 900 K for Si(111) : Cu-'5×5' and about 800 K for the discommensurate phases introcuded by Ga on Si(111) and Ge(111).

c) The discommensurate Ge(111) : Cu phase is, in contrast to Si(111) : Cu-'5×5', only metastable. Upon heating to higher temperatures, it decomposes, the Cu clusters in 3D islands, and the majority of the Ge(111) surface is depleted of Cu and adopts the $c(2 \times 8)$ reconstruction.

d) For the Ge(111) : Cu phase the domain superlattice is aligned along the $\langle 11\bar{2} \rangle$ directions, i.e., rotated 30° with respect to Si(111) : Cu-'5×5' which is aligned along the $\langle 01\bar{1} \rangle$ directions [22, 43]. This rotation is also reflected in the corresponding LEED patterns [16, 38].

e) There is a small though significant difference in the mean Cu adsorption site for Si(111) : Cu-'5×5' and the Ge(111) : Cu phase as determined by XSW.

---

[2]) Surface X-ray diffraction confirmed the 10% mismatch and 3° rotation but showed that the latter is slightly spirally [42].

With respect to a): For the case of Si(111) : Cu-'5×5', the saturation coverage of 1.3 ML means that the internal structure of the domains consists of two Cu atoms per unit cell (substitutional *and* H_3 adsorption sites). In the commensurate limit this would correspond to a saturation coverage of 2 ML. However, the 10% expanded overlayer decreases the saturation coverage to 1.6 ML and the light (i.e., depleted of Cu) domain walls reduce the saturation coverage further to 1.3 ML. For Ge(111) : Cu the saturation coverage is not exactly determined up to now but it is about 0.7 to 0.8 ML and thus certainly less than 1 ML. Consequently, there is basically one Cu atom per 1×1 unit cell which would lead in the commensurate limit to 1 ML saturation coverage. However, from atomically resolved STM images a mismatch of the overlayer (within the domain) of about 5% is deduced which would lead to a saturation coverage of 0.9 ML. Since the overlayer exhibits a positive mismatch (larger lattice constant), the domain walls are expected to be light, decreasing the Cu saturation coverage further.

With respect to b): For the Si(111) : Cu-'5×5' structure to form, the Si atoms of the (111) surface layer are replaced by Cu and the surplus Si atoms, which are the surface atoms *and* the adatoms of the 7×7 structure on which the Cu is deposited, have to diffuse e.g. to step edges. Thus, many bonds have to be broken and quite massive material transport is needed which explains the quite high formation temperature of about 900 K. For the discommensurate Ge(111) : Cu phase it is much lower. From Fig. 12 we can learn that the Ge(111) : Cu structure is formed at around 400 K since P^{111} of Cu exhibits already the value characteristic of this structure. Optimal order is achieved at around 600 K as indicated by the maximum in F^{111}. This low formation temperature is not in agreement with the massive material transport needed for the formation of the '5×5' structure (the whole (111) top layer is removed). This suggests that the microscopic structure of the Ge(111) : Cu reconstruction is different.

With respect to c): Already at 600 K, the Ge(111) : Cu structure starts to decompose as shown by the change in P^{111} and the decrease in F^{111}. The decomposition of the Ge(111) : Cu structure happens along two routes: (i) Cu forms thicker epitaxial layers and 3D islands, most likely consisting of a Cu germanide (cf. Fig. 9e, f and [27]). (ii) Cu diffuses into the Ge bulk. This becomes obvious from Fig. 10c, d. With increasing annealing temperature, it is not possible to achieve a good fit to the Cu fluorescence data using Eq. (2) (cf. Fig. 10c, d). We already stressed that this function will describe the fluorescence yield of *any* foreign atom (Cu in this case) *on* the surface whether a single layer or 3D islands. However, for atoms *within* the bulk of the crystal this functional form is not appropriate. The extinction effect has to be taken into account; i.e., the effect that the X-ray wave propagates within the range of Bragg reflection less deeply into the crystal and thus fewer Cu atoms are excited by the wavefield. Thus, the fluorescence yield of atoms deep (> 100 nm) in the bulk of the substrate will exhibit a *minimum* within the range of total reflection. The yield curve in Fig. 10c and in particular Fig. 10d exhibits this signature and proves that a significant amount of Cu is diffusing deep into the Ge at temperatures $\gtrsim$600 K. In view of the diffusion coefficient this is basically no surprise since it is known to be high for Cu in Ge. However, the solubility is only about $1.7 \times 10^{14}\,\mathrm{cm}^{-3}$ at 850 K [44, 45]. This means that for an extinction depth of roughly 10 µm, i.e., the depth from which we observe the Cu fluorescence within the range of total reflectivity, less than 2×10^{11} solved Cu atoms cm^{-2} ($< 0.1\%$ of 1 ML) could contribute to the signal, a contribution hard to notify. Why the influence of diffused Cu atoms is obviously much stronger

(i.e., there seems to be a much higher concentration of Cu in a depth up to $\approx 10\,\mu m$) is not clear.

With respect to d): The 30° rotation of the Ge(111) : Cu domain superlattice relative to the orientation of the Si(111) : Cu phase is an obvious proof that the structures are quite different. It is the expression of a fundamental difference in the microscopic structure within the interior of the domains.

With respect to e): If the microscopic structure of the Ge(111) : Cu phase would be equivalent to the '5×5' one, a value $P^{11\bar{1}} = 0.66$ would be expected. However, determined by the measurement was $P^{11\bar{1}} = 0.63$, a significantly smaller value and thus another indication that the microscopic structures of the discommensurate phases of Ge(111) : Cu and Si(111) : Cu are different.

A microscopic structure of the discommensurate Ge(111) : Cu phase which is in agreement with all known facts is shown in Fig. 18. The Cu atoms are integrated into the

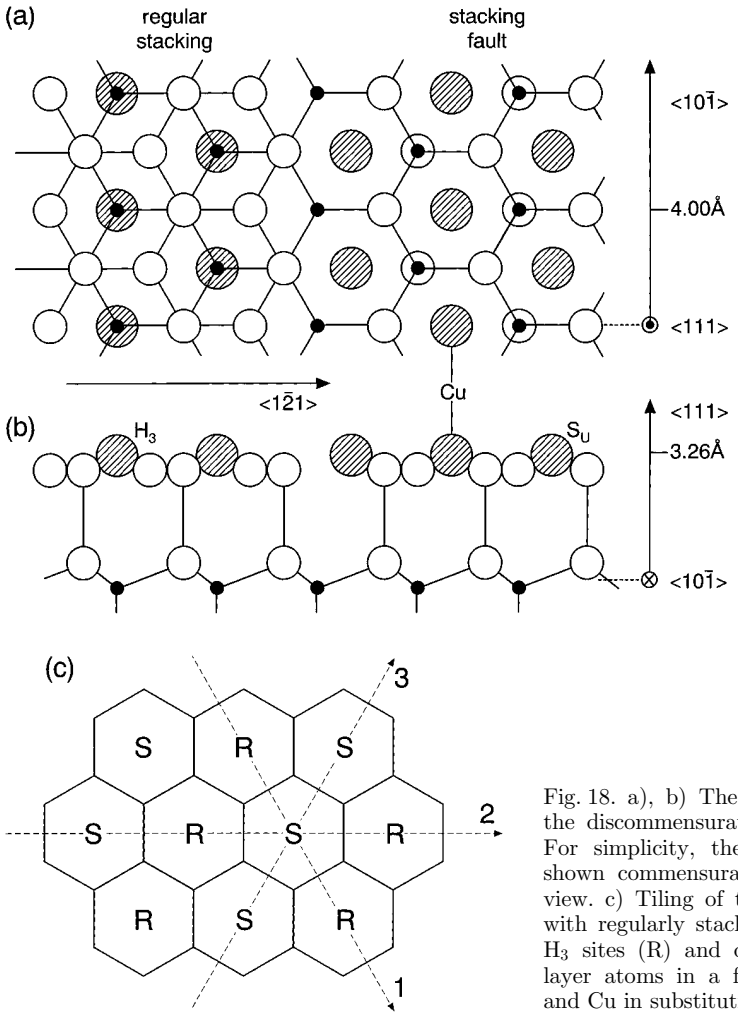

Fig. 18. a), b) The microscopic structure of the discommensurate phase of Ge(111) : Cu. For simplicity, the GeCu surface layer is shown commensurate. a) Topview, b) sideview. c) Tiling of the surface with domains with regularly stacked Ge atoms and Cu in H_3 sites (R) and domains with Ge surface layer atoms in a faulted stacking sequence and Cu in substitutional sites (S)

Ge(111) surface layer. In one type of domains this happens with the Ge surface atoms basically staying in place and the Cu atoms occupying the open, hollow (H_3) site, strongly downward relaxed. In the other type of domains the Cu atoms are in a substitutional position (S_u) and Ge is in the open, hollow site. Ge surface atoms are now about 0.4 Å *below* the surface diffraction plane. All Cu atoms are *within* the surface diffraction plane (i.e., $P^{111} = 0.0$), although a small vertical height difference between the Cu H_3 and S_u positions is consistent with the XSW results. Bond lengths calculated from this model are 2.42 Å for Ge–Ge in the surface layer (bulk Ge: 2.45 Å) and 2.45 Å for Ge–Cu which is 2% smaller than the sum of the metallic Cu radius (1.28 Å) and the covalent Ge radius.

With this model, the measured coherent position $P^{11\bar{1}} = 0.63$ is reproduced exactly if 57% of the Cu atoms are in a stacking fault position (H_3 site) and 43% are in a substitutional position (S_u site). This would lead to $F^{11\bar{1}}_{S,H_3} = 0.51$. The XSW measurement shown in Fig. 10a, b was performed for a Cu coverage higher than the saturation coverage. The excess Cu is most likely contained in 3D Cu clusters and thus will be distributed randomly (incoherently) with respect to the X-ray standing wavefield. Thus, we express the experimentally observed $(11\bar{1})$ coherent fraction as

$$F^{11\bar{1}}_{\text{exp}} = F^{11\bar{1}}_{S,H_3} f_G (1 - U) \,. \tag{12}$$

We can estimate the "uncoherent fraction" U with $F^{111}_{\text{exp}} = (1 - U)$ since from our model follows that $F^{111} = 1.0$ for a Cu coverage below the saturation coverage because we assume all Cu atoms at the same position normal to the surface; an assumption which is certainly oversimplified. From Eq. (12) we calculate $f_G = 0.67$ and thus obtain $\delta P^{11\bar{1}}_{Cu} = 0.14$ for the standard deviation of the distribution of the Cu around the two mean positions.

The proposed model for the discommensurate phase of Ge(111) : Cu can explain the experimental observations, yet, some questions remain open. The STM images show a 4.2 Å hexagonal lattice within the domains, and the protrusions correspond to Cu atoms in regular stacking in one domain and with a stacking fault in the other, in agreement with the XSW results. There is no direct evidence for the Ge layer. There is only indirect evidence: The Cu surface atoms do not from a densely packed layer, thus they must be bound to Ge. If they would be simply adsorbed on top of Ge atoms, the 5% mismatch in plane and the XSW (111) coherent position $P^{111} = 0.0$ could not be explained (with a Ge–Cu bond length of 2.5 Å, $P^{111} = 0.89$ for the top position).

Unclear is the situation at the boundaries between the domains. The reason for the occurrence of the stacking fault is supposedly the same as for the Ge(111) : Ga β-phase: it permits a chemically satisfied bonding situation within the domain walls which thus join in the β-phase always a domain with and without stacking fault (B and A in Fig. 17). For a hexagonal superlattice of domains of two types where one type (R) exhibits regular stacking and the other type (S) a stacking fault it is not possible to have exclusively R/S boundaries, rather there must be boundaries of type R/S, S/S, and R/R (cf. Fig. 18c). Indeed, closer inspection of Fig. 9d, e reveals that the domains are not truly hexagonal. In two directions of the 120° rotated axes of the hexagonal coordinate system the domains are touching. In the third direction, a gap is visible between the domains (cf. e.g. Fig. 9b). Fig. 9e shows that the supercells resemble distorted hexagons with four long and two short sides. Fig. 18c shows the tiling of the surface with two

different domains schematically. In the directions 1 and 2 domains with regular stacking (R) are attached to domains with Ge in a faulty stacking sequence (S). In the third direction 3, there are exclusively S/S and R/R boundaries. This overall appearance is indeed in agreement with the STM images.

4.5 Adsorption of noble metals on (111) Si and Ge surfaces

Silver and gold in the ML range induce commensurate $\sqrt{3} \times \sqrt{3}\,\mathrm{R30}^\circ$ reconstructions on Si(111) and Ge(111). Thus, copper on Si(111) and Ge(111) appears to behave completely different. However, a closer look reveals strong similarities of the surface structures formed by these noble metals. In all these cases, the metal atoms are imbedded in the (111) surface layer. For Ge(111) : Au-$\sqrt{3} \times \sqrt{3}\,\mathrm{R30}^\circ$, the top layer of the (111) surface double layer is removed and Au is basically adsorbed in substitutional positions at $P^{111} \approx 0.07$ [46] but slightly distorted, laterally forming Au trimers [47, 48]. The same structure is meanwhile accepted for Si(111) : Au-$\sqrt{3} \times \sqrt{3}\,\mathrm{R30}^\circ$ [49, 50]. The Si(111) : Ag-$\sqrt{3} \times \sqrt{3}\,\mathrm{R30}^\circ$ reconstruction is similar except that the Si atoms in the AgSi layer form trimers [51] which is also the accepted model for Ge(111) : Ag-$\sqrt{3} \times \sqrt{3}\,\mathrm{R30}^\circ$ [50]. The saturation coverage of all these reconstructions is 1 ML.

All of the three noble d-metals can adopt the valence state 1^+. However, whereas Ag exhibits this state exclusively, Cu and Au can adopt the valence states 2^+ and 3^+, respectively, as well. Simple electron counting suggests that Cu is on Ge(111) in the valence state 1^+ (at least within the domains) if our model is correct. However, we do not know the structure of the domain boundaries for Ge(111) : Cu and Cu may exhibit there a different valence state (2^+). It is not uncommon for Cu to appear in valence state 1^+ *and* 2^+ in a single compound. This might be the case for Si(111) : Cu-'5×5' since a) Cu appears in two different adsorption sites (S_u *and* H_3 at different heights) and b) two Cu atoms will share three Si valence electrons per 1×1 surface unit cell. Different valence states of the metals are certainly one explanation for the different observed structures on (111) and Ge. To what extent a different electronic structure of the Si and Ge surface atoms is responsible for the different Cu induced structures or whether differences are mostly strain related because of the 4% difference in Si and Ge lattice constants still needs to be explored.

4.6 Ge(111) : In

The "striped" phase of Ge(111) : In is unique among the discussed systems. The reconstruction is commensurate along the stripes but not in the orthogonal direction and breaks the threefold symmetry of the (111) surface. The In atoms are located in the dark stripes and adsorbed in S_u substitutional sites exclusively, as the XSW results clearly show (cf. Fig. 14a, b and Fig. 15a). Since the In is relaxed significantly downward (0.4 Å) compared to an ideal substitutional position there must be severe stress in the surface layer and the In laterally relaxed and moved away from the high symmetry site. The in-plane coherent fraction $F^{11\bar{1}} = 0.66$ suggests a standard deviation of the (Gaussian) distribution of $\delta P^{11\bar{1}} = 0.13$ (i.e. $\sigma = 0.45$ Å in the $\langle 11\bar{1} \rangle$ direction, corresponding to $\sigma = 0.48$ Å in-plane), assuming $F^{111}_{\mathrm{exp}} = 0.9 = (1 - U)$. In other words, the In atoms in the substitutional sites must have caused locally a significant expansion of the surface lattice. At present there is not enough experimental evidence to determine the In

induced structure in the dark stripes with confidence. A possible model is suggested by Gai et al. [52]. However, since the authors assume In to be present in regular substitutional sites it is not in agreement with the XSW results.

There are several "hexagonal" phases reported for Ge(111) : In [6, 52]. Shown in Fig. 13d is the $4\sqrt{3} \times 4\sqrt{3}$ reconstruction for which the XSW measurements (Fig. 14c, d) were carried out. Other reported phases are $4.3\sqrt{3}$ and $4.2\sqrt{3}$, which are most likely very similar to the $4\sqrt{3}$ structure, except that the domain superlattice is not periodic, and the $\sqrt{31} \times \sqrt{31}$ structure. For all these phase the In coverage is almost the same.

The XSW results (cf. Fig. 14c, d and Fig. 15b) prove that In is adsorbed in the substitutional site in both the regular *and* the faulted geometry. The P^{111} and $P^{\bar{1}\bar{1}\bar{1}}$ values suggest that 65% of the In atoms are in regular substitutional sites and 35% of the In atoms are in substitutional sites in a faulted stacking sequence. This reproduces the experimentally observed $P^{11\bar{1}}$ value and yields $F^{111}_{\mathrm{S,SF}} = 0.57$ in the commensurate limit. Setting $F^{111}_{\mathrm{exp}} = f_{\mathrm{G}}(1-U)\, F^{11\bar{1}}_{\mathrm{S,SF}}$, where we obtain $f_{\mathrm{G}} = 0.69$ and thus $\delta P^{11\bar{1}} = 0.14$ (i.e., $\sigma = 0.48$ Å normal to the $(11\bar{1})$ plane, i.e., $\sigma = 0.51$ Å in-plane) for the standard deviation of the (assumed) Gaussian distribution around the two mean adsorption sites. The individual (small) domains of the $4\sqrt{3}$ phase seem to contain only six to eight In atoms. Assuming that the internal lattice constant of the domains is determined by the sum of the covalent radii of In (1.44 Å) and Ge (1.22 Å) with a practically unbuckled surface layer leads to $a_{\mathrm{InGe}} = 4.6$ Å, i.e. a 15% increase compared to $a_{\mathrm{Ge}} = 4.0$ Å. With this lattice constant and an average domain size with seven In atoms, where the central In atom is at the high symmetry substitutional site, the experimentally observed coherent fraction can be reproduced. Since the domains are very small, the internal lattice constant is difficult to determine with sufficient accuracy with the STM. The value of 5 Å, suggesting a 25% increase, given in [39] is certainly overestimated. The 15% increase given in [52] appears to be more realistic and agrees with our present findings.

Gai et al. [52] also suggest a model for the $4\sqrt{3}$ reconstruction. However, since they assume In in regular subtitutional sites exclusively it is not correct. The XSW results show that 1/3 of the In is in the faulted substitutional sites which suggests that 1/3 of the domains contain In in faulted substitutional sites. This in turn suggests that the domain superlattice consists of three different types of domains as shown in Fig. 19; one type contains In in faulted positions (S) the other two (R and R′) in regular substitutional positions. The distance between the individual domains is $\approx 4a_{\mathrm{Ge}}$ as determined with STM. However, as shown in Fig. 19, because the superlattice consists of three different types of domains (with different structure) the repeat distance of the domain superlattice is $4\sqrt{3}a_{\mathrm{Ge}}$ in agreement with the diffraction pattern. On the long range, the $4\sqrt{3}$ structure resembles an almost ideal, hexagonal superlattice (cf. Fig. 13c) whereas the closeup look in Fig. 13d shows that the individual domains are not really hexagonal.

4.7 Comparison with Frenkel-Kontorova, Frank-van der Merwe discommensuration

The system Si(111) : Cu-'5×5' can be turned "upside down". A hexagonal Cu_2Si layer also forms if Si is deposited on the Cu(001) surface [53]. The structure is slightly distorted but the hexagonal 2D Cu_2Si layer exhibits long-range structural integrity. The surface layer is basically incommensurate with the Cu substrate but mildly modulated with the substrate (001) surface potential, resulting in a high-order commensurability as

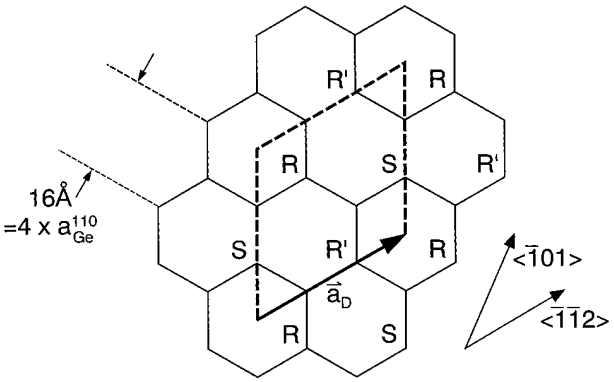

Fig. 19. Schematic model of the Ge(111) : In-4 $\sqrt{3} \times 4\sqrt{3}$R30° superlattice with the surface tiled by three different domains with In in regular stacking sequence (R, R′) and faulted stacking sequence (S). The exact hexagonal shape of the domains is an idealization (cf. Fig. 13d)

concluded from diffraction results. The overlayer exhibits a structure which is basically expected from the FK/FvdM model.

The systems discussed throughout this paper display new, unique features which are mostly due to the strong and directional covalent bonding on semiconductor surfaces in which case the assumption in the FK/FvdM theory of a sinusoidally modulated substrate potential is a poor approximation. As a consequence, the adsorbate will no longer resemble a homogeneous, incommensurate overlayer slightly modulated by the substrate. Instead, completely different bond characters and topologies may appear locally. This will predominantly show up in the domain boundaries. In fact, the energetic situation within the domain boundaries can even dictate the appearance of new phases; the system Ge(111) : Ga is here an illustrative example.

Total energy calculations proved that of all adsorbate positions the substitutional site was the energetically most favorable for Ga on Ge(111) and Si(111) for ML coverage whereas the substitutional site in a faulted stacking sequence was higher in energy by ≈ 0.1 eV. This situation does not change if the ovelayer is strained, although a reduction of the surface energy be more than 0.4 eV per 1×1 unit cell was calculated for Ge(111) : Ga with an expansive strain of $\approx 10\%$ [28].

With these basic facts the Ge(111) γ-phase can be understood in terms of the FK/FvdM scheme. Ga is basically in the substitutional position. However, the GeGa layer has an increased equilibrium lattice constant, but the overlayer does not become simply incommensurate since the bonds to the substrate are too strong. Instead, the overlayer becomes discommensurate: In the center of the domains the overlayer is almost in registry with the substrate. Toward the periphery of the domains, registry with the substrate decays and is lost completely at the domain boundaries. The mismatch of the GeGa overlayer with the substrate is positive and consequently the discommensurations are depleted of Ga.

While this general appearance of the γ-phase can be qualitatively understood within the FK/FvdM theory the appearance of the β-phase cannot. Here, about 40% of the Ga is adsorbed in faulted substitutional sites, a position which is ≈ 0.1 eV less favorable in energy compared to the regular stacking. However, STM revealed a large number of dangling bonds (DB) at the domain boundary of the γ-phase [27] – about 1 DB at the boundary per five atoms in the interior of the domains. One DB "costs" roughly 1 eV in energy [54]. With the help of the stacking fault, DBs at the boundaries of domains with

regular and faulted stacking can be avoided [27]. Just using these approximations for the energies and neglecting other energetic contributions (such as strain) it can be understood in a crude estimate that the generation of the stacking fault can be energetically favorable since five atoms in the stacking fault position cost together ≈ 0.5 eV, but by eliminating one DB the surface can gain ≈ 1 eV. In other words, a changed, more favorable bonding topology within the discommensurations determines the stability of a new structure – a mechanism which cannot be understood within the framework of the FK/FvdM theory. The surface energy and stability of the Ga induced phases on Si(111) and Ge(111) are discussed in detail in [28].

5. Conclusions

The discussed surface phases are characterized by superlattices of domains. Except for the $4\sqrt{3} \times 4\sqrt{3}\,\mathrm{R}30^\circ$ phase of Ge(111) : In they are nonperiodic. Despite the lack of translational symmetry, the superlattices basically reflect the threefold rotational symmetry of the (111) surface (except for the Ge(111) : In striped phase). The large scale and the lack of long-range order of these reconstructions renders a structural analysis with traditional surface probes difficult, in particular with diffraction techniques.

Using STM we have learned about the topography and electronic properties of these systems on the nm scale. It is a characteristic and unique feature of these reconstructions, that they are electronically strongly inhomogeneous. The electronic structure of the domain walls can differ strikingly from the electronic structure of the interior of the domains. E.g. for the Ge(111) : Ga γ-phase, the discommensurations exhibit a higher density of DBs and will thus most likely be metallic whereas all DBs are saturated in the interior of the domains and they thus are expected to exhibit little density of states within the bulk bandgap.

For all these reconstructions the XSW technique provides information about the principal adsorption site of the metal atoms: substitutional or/and faulted substitutional (relaxed H_3). The XSW technique furthermore provides a very stringent test whether an adsorbate exhibits a commensurate, incommensurate or strongly modulated incommensurate reconstruction [55] because the XSW technique probes sensitively the *correlation* of the adsorbate with the substrate lattice. For all the analyzed systems it turns out that, while the basic adsorption sites are rather simple, strain leads to a complex structure with a rather wide distribution around the mean adsorption site.

Many questions regarding these reconstructions have been answered but many others remain open. A particularly challenging question is the microscopic structure of the domain walls of all the phases presented here. Also the superstructure of In in the striped phase of Ge(111) : In remains to be determined. Furthermore, the question arises whether all these reconstructions are in the ground state at room temperature since most of them are nonperiodic or whether they are "frozen in" at some higher temperature because of the lack of surface diffusion. Here the Ge(111) : Cu discommensurate phase is unique since it is a) metastable and b) may even exhibit a phase transition below room temperature. Unfortunately, theory cannot be of much help at present to answer these questions because the scale of these reconstructions is too large and the nonperiodicity is a big stumbling block.

Future research on these fascinating systems may address challenging problems such as temperature and coverage driven phase transitions as well as the possible influence of

entropy at elevated temperature e.g. in view of domain wall fluctuation. These problems have been extensively discussed for classical discommensurate systems such as rare gases on graphite [56] and it is task for the future to sort our similarities and dissimilarities with discommensurate systems on semiconductors surfaces.

Acknowledgements Many valuable discussions with Emilio Artacho, Mark Hybertsen, Jim Patel, Wolfgang Moritz, Niels Christensen, Axel Svane, Manuel Cardona and numerous other colleagues are gratefully acknowledged. Furthermore we like to thank Gerhard Scherb for valuable suggestions after carefully reading the manuscript. This work was supported by the German BMBF under contract No. 05-622GUA and in part by the US Department of Energy under contract No. W-31-109-ENG-38 to Argonne National Laboratory. We like to thank the staff of the National Synchrotron Light Source for providing the X-ray beam and for assistance on the floor. The NSLS is supported by the United States Department of Energy under contract No. DE-AC02-76CH00016.

References

[1] J. P. La Femina, Surf. Sci. Rep. **16**, 133 (1992).
[2] W. Mönch, Semiconductor Surfaces and Interfaces, Springer-Verlag, 1993.
[3] J. J. Lander and J. Morrison, Surf. Sci. **2**, 553 (1964).
[4] M. Otsuka and T. Ichikawa, Jap. J. Appl. Phys. **24**, 1103 (1985).
[5] J. T. Grant and T. W. Haas, Surf. Sci. **23**, 347 (1970).
[6] T. Ichikawa, Surf. Sci. **111**, 227 (1981).
[7] J. C. Hansen, B. J. Knapp, R. de Sonza-Machado, M. K. Wagner, and J. G. Tobin, J. Vac. Sci. Technol. A **7**, 2083 (1989).
[8] J. Zegenhagen and P. Molinàs-Mata, Ultramicr. **42/44**, 952 (1992).
[9] G. Binnig, H. Rohrer, Ch. Gerber, and E. Weibel, Phys. Rev. Lett. **49**, 57 (1982).
[10] P. L. Cowen, J. A. Golovchenko, and M. F. Robbins, Phys. Rev. Lett. **44**, 1680 (1980).
[11] B. W. Batterman, Phys. Rev. **133**, A759 (1964).
[12] J. Zegenhagen, M. S. Hybertsen, P. E. Freeland, and J. R. Patel, Phys. Rev. B **38**, 7885 (1988).
[13] D. M. Chen, J. A. Golovchenko, P. Bedrossian, and K. Mortensen, Phys. Rev. Lett. **61**, 2867 (1988).
[14] J. R. Patel, J. Zegenhagen, P. E. Freeland, M. S. Hybertsen, J. A. Golovchenko, and D. M. Chen, J. Vac. Sci. Technol. B **7** 894 (1989).
[15] E. Daugy, P. Mathiez, F. Salvan, and J. M. Layet, Surf. Sci. **154**, 267 (1985).
[16] H. Kemmann, F. Müller, and H. Neddermeyer, Surf. Sci. **192**, 11 (1987).
[17] R. B. Doak and D. B. Nguyen, Phys. Rev. B **40**, 1495 (1989).
[18] K. Takayanagi, Y. Tanishiro, T. Ishitsuka, and K. Akiyama, Appl. Surf. Sci. **41/42**, 337 (1989).
[19] R. J. Wilson and S. Chiang, Phys. Rev. B **38**, 12696 (1988).
[20] J. E. Demuth, U. K. Koehler, R. J. Hamers, and P. Kaplan, Phys. Rev. Lett. **62**, 641 (1989).
[21] K. Mortensen, Phys. Rev. Lett. **66**, 461 (1991).
[22] J. Zegenhagen, E. Fontes, F. Grey, and J. R. Patel, Phys. Rev. B **46**, 1860 (1992).
[23] P. Molinàs-Mata, M. Böhringer, and J. Zegenhagen, Surf. Sci. **317**, 378 (1994).
[24] M. Böhringr, P. Molinàs-Mata, J. Zegenhagen, G. Falkenberg, L. Seehofer, L. Lottermoser, R. L. Johnson, and R. Feidenhans'l, Phys. Rev. B **52**, 1948 (1995).
[25] P. Molinàs-Mata, M. Böhringer, E. Artacho, J. Zegenhagen, L. Seehofer, T. Buslaps, R. L. Johnson, E. Findeisen, R. Feidenhans'l, and M. Nielsen, phys. stat. sol. (a) **148**, 191(1995).
[26] E. Artacho, P. Molinàs-Mata, M. Böhringer, J. Zegenhagen, G. E. Franklin, and J. R. Patel, Phys. Rev. B **51**, 9952 (1995).

[27] M. Böhringer, P. Molinàs-Mata, E. Artacho, and J. Zegenhagen, Phys. Rev. B **51**, 9965 (1995).
[28] E. Artacho and J. Zegenhagen, Phys. Rev. B **52**, 16373 (1995).
[29] J. Zegenhagen, J. R. Patel, P. Freeland, D. M. Chen, J. A. Golovchenko, P. Bedrossian, and J. E. Northrup, Phys. Rev. B **39**, 1298 (1989).
[30] J. Zegenhagen, E. Artacho, P. E. Freeland, and J. R. Patel, Phil. Mag. B **70**, 731, (1994).
[31] see e.g.: J. Kraft, M. G. Ramsey, and F. P. Netzer, Phys. Rev. B **55**, 5384 (1997) and references therein.
[32] M. Yoshimura, K. Takaoka, T. Yoa, T. Sato, T. Sueyoshi, and M. Iwatsuki, Mater. Res. Soc. Symp. Proc. **195**, 157 (1993).
[33] J. Frenkel and T. Kontorova, Phys. Z. SU **13**, 1 (1938).
[34] F. C. Frank and J. H. von der Merwe, Proc. Roy. Soc. London **189**, 205 (1949).
[35] J. Zegenhagen, Surf. Sci. Rep. **18**, 199 (1993).
[36] J. Zegenhagen, G. Materlik, and W. Uelhoff, J. X-Ray Sci. Technol. **2**, 214 (1990).
[37] J. Zegenhagen, J. Phys.: Condensed Matter **5**, A 89 (1993).
[38] M. Böhringer, Q. D. Jiang, R. Berndt, W. Schneider, and J. Zegenhagen, Surf. Sci. **367**, 245 (1996).
[39] M. Böhringer and J. Zegenhagen, Surf. Sci. **327**, 248 (1995).
[40] J. Zegenhagen, Physica Scripta **T39**, 328 (1991).
[41] J. Zegenhagen, J. R. Patel, and E. Fontes, Appl. Surf. Sci. **60/61**, 505 (1992).
[42] F. Grey, R. Feidenhans'l, M. Nielsen, R. L. Johnson, and J. Zegenhagen, unpublished.
[43] D.-M. Chen, unpublished results.
[44] N. A. Stolwijk, W. Frank, J. Hölzl, S. J. Pearton, and E. E. Haller, J. Appl. Phys. **57**, 5211 (1985).
[45] H. Bracht, N. A. Stolwijk, and H. Mehrer, Phys. Rev. B **43**, 14465 (1991).
[46] M. J. Bedzyk, S. M. Durbin, and L. E. Berman, Bull. Am. Phys. Soc. **31**, 668 (1986).
[47] P. B. Howes, C. Norris, M. S. Finney, E. Vlieg, and R. G. van Silfhout, Phys. Rev. B **48**, 1632 (1993).
[48] H. Over, C. P. Wang, and F. Jona, Phys. Rev. B **51**, 4231 (1995).
[49] D. Dornisch, W. Moritz, H. Schulz, R. Feidenhans'l, M. Nielsen, F. Grey, and R. L., Johnson, Phys. Rev. B **44**, 11221 (1991).
[50] H. Huang, H. Over, S. Y. Tong, J. Quinn, and F. Jona, Phys. Rev. B **49**, 13483 (1994).
[51] see e.g., T. Takahaski and S. Nakatani, Surf. Sci. **282**, 17 (1993) and references therein.
[52] Z. Gai, R. G. Zhao, Y. He, H. Ji, C. Hu, and W. S. Yang, Phys. Rev. B **53**, 1539 (1996).
[53] A. P. Graham, B. J. Hinch, G. P. Kochanski, E. M. McCash, and W. Allison, Phys. Rev. B **50**, 15304 (1994).
[54] see e.g., J. L. Mercer and M. Y. Chou, Phys. Rev. B **48**, 5374 (1993) and references therein.
[55] G. C. La Rocca and J. Zegenhagen, Phys. Rev. B **44**, 13666 (1991).
[56] see e.g., J. Villain, in: Ordering in Strongly Fluctuating Condensed Matter Systems, Ed. T. Riste, Plenum Press, New York 1980.
P. Bak, in: Chemistry and Physics of Solid Surfaces V, Ed. R. Vanselow and R. Howe, Springer-Verlag, Heidelberg 1984.
S. N. Coppersmith, D. S. Fisher, B. I. Halperin, P. A. Lu, and W. F. Brinkman, Phys. Rev. B **25**, 349 (1982).